



HAL
open science

P-selectin targeted RAGE-shRNA lipoplexes alleviate atherosclerosis-associated inflammation

Cristina Ana Mocanu, Elena Valeria Fuior, Geanina Voicu, Daniela Rebleanu, Florentina Safciuc, Mariana Deleanu, Ioana Madalina Fenyo, Virginie Escriou, Ileana Manduteanu, Maya Simionescu, et al.

► To cite this version:

Cristina Ana Mocanu, Elena Valeria Fuior, Geanina Voicu, Daniela Rebleanu, Florentina Safciuc, et al.. P-selectin targeted RAGE-shRNA lipoplexes alleviate atherosclerosis-associated inflammation. Journal of Controlled Release, 2021, 338, pp.754 - 772. 10.1016/j.jconrel.2021.09.012 . hal-03407602

HAL Id: hal-03407602

<https://cnrs.hal.science/hal-03407602>

Submitted on 28 Oct 2021

HAL is a multi-disciplinary open access archive for the deposit and dissemination of scientific research documents, whether they are published or not. The documents may come from teaching and research institutions in France or abroad, or from public or private research centers.

L'archive ouverte pluridisciplinaire **HAL**, est destinée au dépôt et à la diffusion de documents scientifiques de niveau recherche, publiés ou non, émanant des établissements d'enseignement et de recherche français ou étrangers, des laboratoires publics ou privés.



P-selectin targeted RAGE-shRNA lipoplexes alleviate atherosclerosis-associated inflammation

Cristina Ana Mocanu^a, Elena Valeria Fuior^a, Geanina Voicu^a, Daniela Rebleanu^a, Florentina Safciuc^a, Mariana Deleanu^b, Ioana Madalina Fenyo^c, Virginie Escriou^d, Ileana Manduteanu^a, Maya Simionescu^a, Manuela Calin^{a,*}

^a “Medical and Pharmaceutical Bionanotechnologies” Laboratory, Institute of Cellular Biology and Pathology “Nicolae Simionescu” of the Romanian Academy, 050568 Bucharest, Romania

^b “Liquid and Gas Chromatography” Laboratory, Institute of Cellular Biology and Pathology “Nicolae Simionescu” of the Romanian Academy, 050568 Bucharest, Romania

^c “Gene Regulation and Molecular Therapies” Laboratory, Institute of Cellular Biology and Pathology “Nicolae Simionescu” of the Romanian Academy, 050568 Bucharest, Romania

^d Université de Paris, UTCBS, CNRS, INSERM, F-75006 Paris, France

ARTICLE INFO

Keywords:
Atherosclerosis
Lipoplexes
P-selectin
RAGE
shRNA

ABSTRACT

The receptor for advanced glycation end products (RAGE) plays a central role in the chronic inflammatory process associated with atherosclerosis development. We aimed to develop lipoplexes carrying RAGE-short hairpin (sh) RNA, targeted to the adhesion molecule P-selectin, selectively expressed on the surface of activated endothelium (Psel-lipo/shRAGE) to down-regulate RAGE expression as a therapeutic strategy for atherosclerosis. In vitro, Psel-lipo/shRAGE lipoplexes were efficiently taken up by activated endothelial cells (EC), decreased the expression of RAGE protein, and proved to be functional by reducing the monocyte adhesion to activated EC. In ApoE-deficient mice, the targeted lipoplexes accumulated specifically and efficiently transfected the aorta. The repeated administration of Psel-lipo/shRAGE lipoplexes, twice per week for one month: i) reduced the expression of RAGE protein in the aorta by decreasing the expression of NF- κ B and TNF- α ; ii) diminished the plasma levels of TNF- α , IL6, IL-1 β , and MCP-1; iii) inhibited the atherosclerotic plaque development and iv) had no significant adverse effects. In conclusion, the newly developed Psel-lipo/shRAGE lipoplexes reduce the inflammatory processes associated with RAGE signaling and the progression of atherosclerosis in ApoE-deficient mice. Downregulation of RAGE employing these lipoplexes may represent a promising new targeted therapy to block atherosclerosis progression.

Abbreviations: ALP, alkaline phosphatase; ALT, alanine aminotransferase; ApoE, apolipoprotein E; AST, aspartate aminotransferase; BUN, Blood urea nitrogen; DAPI, 4',6-diamidino-2-phenylindole; DMAPAP, 2-{3-[Bis-(3-amino-propyl)-amino]-propylamino}-N-ditetradecyl carbamoyl methyl-acetamide; DMEM, Dulbecco's modified Eagle's medium; DOPE, 1,2-dioleoyl-sn-glycero-3-phosphoethanolamine; EC, endothelial cells; EDTA, ethylenediaminetetraacetic acid; FACS, fluorescence-activated cell sorting; H&E staining, hematoxylin and eosin staining; HFD, high-fat diet; IL-6, interleukin-6; IVIS, in vivo imaging system; LPS, lipopolysaccharides; Mac-1, macrophage-1 antigen; Mal-PEG-DSPE, 1,2-distearoyl-sn-glycero-3-phosphoethanolamine-N-[maleimide(polyethylene glycol)-2000]; MCP-1, monocyte chemoattractant protein 1; NBD-PE, 1,2-dipalmitoyl-sn-glycero-3-phosphoethanolamine-N-(7-nitro-2-1,3-benzoxadiazol-4-yl); NF- κ B, nuclear factor- κ B; pEYFP, plasmid encoding the green/yellow fluorescent protein derived from *Aequorea Victoria*; Psel-lipo/shCTR lipoplexes, P-selectin-targeted cationic PEGylated liposomes complexed with shCTR plasmid; Psel-lipo/shRAGE lipoplexes, P-selectin-targeted cationic PEGylated liposomes complexed with RAGE-shRNA plasmid; RAGE, receptor for advanced glycation end products; RAGE-shRNA, plasmids containing shRNA sequence specific for RAGE; Rhodamine B-PE, 1,2-dipalmitoyl-sn-glycero-3-phosphoethanolamine-N-(lissamine Rhodamine B sulfonyl); RNAi, RNA interference; Scr-lipo/shRAGE lipoplexes, non-targeted cationic PEGylated liposomes complexed with RAGE-shRNA; shCTR, MISSION® pLKO.1-puro Non-Mammalian shRNA Control Plasmid DNA; shRNA, short hairpin RNA; siRNA, small interfering RNA; TNF- α , Tumor Necrosis Factor- α ; VCAM-1, Vascular Cell Adhesion Molecule 1; λ_{em} , emission wavelength; λ_{ex} , excitation wavelength.

* Corresponding author at: “Medical and Pharmaceutical Bionanotechnologies” Laboratory, Institute of Cellular Biology and Pathology “Nicolae Simionescu” of the Romanian Academy, 050568 Bucharest, Romania.

E-mail address: manuela.calin@icbp.ro (M. Calin).

<https://doi.org/10.1016/j.jconrel.2021.09.012>

Received 31 May 2021; Received in revised form 3 September 2021; Accepted 10 September 2021

Available online 14 September 2021

0168-3659/© 2021 The Author(s).

Published by Elsevier B.V. This is an open access article under the CC BY-NC-ND license

(<http://creativecommons.org/licenses/by-nc-nd/4.0/>).

1. Introduction

The development of an atherosclerotic plaque in the arteries is promoted and sustained by a chronic inflammatory process [1]. Among the receptors with a pivotal role in the onset and progression of the vascular inflammation, the receptor for advanced glycation end products (RAGE) is overexpressed by the activated endothelium, smooth muscle cells and macrophages infiltrated into the atherosclerotic lesions [2–5].

RAGE is a transmembrane receptor that binds to multiple ligands, either endogenous, such as advanced glycation end products (AGEs), high mobility group box (HMGB)-1, S100/calgranulin proteins (such as S100A12 and S100B), amyloid- β peptide (A β), Macrophage-1 antigen (Mac-1) or exogenous (e.g. bacterial endotoxin and microbial DNA) [3,5]. Upon binding of its ligands, endothelial RAGE activates several signal transduction cascades that converge at nuclear factor- κ B (NF- κ B), resulting in the production of proinflammatory cytokines, chemokines, and cell adhesion molecules with the concurrent upregulation of RAGE itself that favor the adhesion of circulating leukocytes, ensuing the amplification of the vascular inflammation [4–7]. RAGE is also functioning as an endothelial adhesion receptor recognized by the leukocyte integrin Mac-1, thus promoting leukocyte recruitment in the arterial wall [8,9]. Previous data have shown that RAGE overexpression by macrophages contributes to the destabilization of the atherosclerotic plaque by inducing the expression of metalloproteinases [10].

The blockade or the absence of RAGE attenuates leukocyte recruitment and decreases the expression of proinflammatory mediators, stabilizing the established atherosclerotic plaque in diabetic ApoE-deficient mice [11,12]. Therefore, RAGE downregulation could represent a therapeutic target to impede atherosclerosis progression [11,13].

Several therapeutic agents used in the treatment of atherosclerosis and diabetes were identified to downregulate RAGE expression, namely statins, angiotensin II-receptor blockers, ω -3 polyunsaturated fatty acids, and thiazolidinediones [14–20]. To date, some synthetic small-molecule inhibitors such as liraglutide, the glucagon-like peptide-1 (GLP-1) analog [21], or inhibitors binding to the three regions of the Ig-like V-type RAGE domain (one example is azeliragon, 3-(4-{2-butyl-1-[4-(4-chlorophenoxy)-phenyl]-1H-imidazole-4-yl}-phenoxy)-propyl]-diethylamine) used both *in vitro* and *in vivo* have been reported to inhibit RAGE by competition, to block the inflammatory process and even to lower the atherosclerotic burden [22].

In an attempt to reduce the vascular inflammation in atherosclerosis, we aimed at finding a more specific method to down-regulate RAGE expression. The RNA interference (RNAi) mechanisms, which serve as a cellular defense against viruses and as epigenetic regulators, represent a therapeutic strategy for selective gene silencing [23]. Of the RNAi strategies used so far for gene therapy, short hairpin RNAs (shRNA) have the advantage of prolonged silencing effect and relatively low cost [24], and are proven to be more potent down-regulators of gene expression as compared to small interfering RNAs (siRNA) [25].

Once delivered into the cell, shRNA is transcribed by the nucleus and transported into the cytosol, where it is processed into siRNA to recognize, bind and finally degrade the targeted mRNA [26]. A comparison side-by-side between shRNA and siRNA reveals that although the mechanism of action of siRNA and shRNA is similar (both act by binding the mRNA of a target gene), shRNA has the advantage of being a renewable source. Thus, on the one hand, shRNA is encoded by plasmids or lentiviral particles that can be easily multiplied in the laboratory by standard techniques, and, on the other hand, once intracellularly delivered, the transfected cells manufacture the siRNA [27]. In addition, previous reports showed that shRNA produces a higher gene knockdown and fewer off-target effects, explained by the fact that it is processed by the endogenous RNAi machinery of the cell, compared to siRNA [25,28,29]. To achieve comparable knockdown efficiencies, higher concentrations and frequent dosing of siRNA are required [27].

In vivo, RNAi faces the challenge of low transfection efficiency since the naked RNAi molecules, once injected into the bloodstream, may be

degraded both extracellularly and intracellularly. Thus, appropriate nanocarriers are needed to protect and transport RNAi to the target tissue and across the cell membrane into the cytosol. This nanocarriers-based delivery strategy also aids in using lower doses and minimizing the side effects, which often include leukopenia, thrombocytopenia, increased synthesis of cytokines (TNF- α , IL-12, IL-6 and IFN- γ), and elevated serum transaminases activity [30,31].

To ensure the specific delivery of the RNAi molecules to the atherosclerotic plaque, we designed nanocarriers directed towards the cell adhesion molecule P-selectin, overexpressed by the activated endothelium during atherosclerosis progression. P-selectin has been used as a reliable target to deliver therapeutic agents to tumors [32,33] and to the lungs of mice with lipopolysaccharides (LPS)-induced acute inflammation [34]. Also, we have reported that P-selectin binding peptide tagged PEGylated lipoplexes bind and efficiently deliver siRNA cargo to activated endothelial cells (EC) [35].

In this study, we hypothesize that suppression of RAGE expression and its downstream pathways using RNAi mediated by nanotechnology approaches may represent a reliable therapeutic strategy to reduce the vascular inflammation in atherosclerosis. To specifically inhibit RAGE signaling at inflammatory sites, we proposed to deliver shRNA sequences, specific for RAGE silencing, to the developing atherosclerotic plaque using as vehicles P-selectin-targeted cationic PEGylated liposomes (Psel-lipo/shRAGE lipoplexes). We present herein the design, preparation and characterization of the Psel-lipo/shRAGE lipoplexes and demonstrate their effects *in vitro* and *in vivo*. We report that the specific downregulation of RAGE in cultured murine EC reduces the monocyte adhesion to the activated EC. After intravenous (*i.v.*) administration in ApoE-deficient mice kept on a high-fat diet (HFD), the P-selectin targeted lipoplexes accumulated preferentially at sites of atherosclerosis in the aorta as compared to non-targeted lipoplexes. Moreover, the administration of P-selectin targeted lipoplexes, carrying a plasmid encoding a fluorescent protein, induced the expression of the protein in the aorta. The administration of Psel-lipo/shRAGE lipoplexes downregulated RAGE expression in the aorta by diminishing the NF- κ B and TNF- α levels and reduced atherosclerosis. The lipoplexes administration did not significantly alter the weight and the hepatic and renal function of the mice.

The current study is the first to identify that shRNA sequences targeting RAGE, protected by nanocarriers directed towards P-selectin, reach the atherosclerotic plaque and reduce its progression.

2. Materials and methods

2.1. Reagents

The main reagents and supplies used in the experiments were purchased from the following sources: Dulbecco's modified Eagle's medium (DMEM), plasmids MISSION® shRNA specific for mouse RAGE (catalog no. SHCLND-NM_007425, the clones from The RNAi Consortium (TRC) Version 1 library TRCN0000071743; TRCN0000071744; TRCN0000071745; TRCN0000071746; TRCN0000071747), MISSION® pLKO.1-puro Non-Mammalian shRNA Control Plasmid DNA and GenElute-Plasmid Midiprep kit were from SIGMA-Aldrich (Merck KGaA, Darmstadt, Germany), tris-(2-carboxyethyl) phosphine (TCEP), XTT (2,3-bis-(2-methoxy-4-nitro-5-sulfophenyl)-2Htetrazolium-5-carboxanilide) Cell Proliferation Kit, fetal bovine serum (FBS), penicillin and streptomycin from Gibco (ThermoFisher Scientific, Waltham, Massachusetts, USA); cell culture dishes were from TPP® (Trasadingen, Switzerland); 1,2-Dioleoyl-sn-glycero-3-phosphoethanolamine (DOPE), 1,2-distearoyl-sn-glycero-3-phosphoethanolamine-N-[maleimide(polyethylene glycol)-2000] (Mal-PEG-DSPE), 1,2-dipalmitoyl-sn-glycero-3-phosphoethanolamine-N-(7-nitro-2-1,3-benzoxadiazol-4-yl) (ammonium salt) (NBD-PE) and 1,2-dipalmitoyl-sn-glycero-3-phosphoethanolamine-N-(lissamine Rhodamine B sulfonyl) (ammonium salt) (Rhodamine B-PE) from Avanti Polar Lipids (Alabaster, AL, USA);

cationic lipid 2-(3-[Bis-(3-amino-propyl)-amino]-propylamino)-N-ditetradecyl carbamoyl methyl-acetamide (DMAPAP) was synthesized as previously described [36]; Amicon centrifugal filter columns (cut-off 100 kDa) from Millipore (Billerica, MA, USA); Spectra/Por dialysis bags (cut-off 500–1000 Da) from Spectrum Labs (Spectrum Europe BV, Breda, Netherlands); peptide with high affinity for P-selectin (H₂N-CKKKKLVSVLDLEPLDAAWL-COOH) and the scrambled peptide (H₂N-CKKKKLLSAVLWDELVDPLA-COOH) were synthesized by GeneCust (Dudelange, Luxembourg); mouse DuoSet ELISA (Enzyme-linked immunosorbent assay) kits for IL-1 β , TNF- α , IL-6 and MCP-1 were from R&D Systems (Minneapolis, MN, USA); antibodies: anti-RAGE (A-9) (cat no. sc-365,154) and anti-tumor necrosis factor (TNF)- α (cat no. sc8301) from Santa Cruz Biotechnology (cat no. sc8301), Anti-nuclear factor- κ B (NF- κ B) p65 and anti-beta tubulin from Abcam (cat no. ab6046) and anti-GAPDH (Ambion cat. no. AM4300) from ThermoFisher Scientific (Ambion cat. no. AM4300); the plasmid that encodes the Enhanced Yellow Fluorescent Protein (pEYFP) was purchased from Clontech Laboratories Inc. (Mountain View, CA, USA).

2.2. Preparation of P-selectin targeted lipoplexes carrying shRNA plasmids

Cationic Liposomes.

The P-selectin binding peptide, sequence H₂N-CKKKKLVSVLDLEPLDAAWL-COOH [37], was coupled to cationic liposomes composed of DMAPAP, DOPE and a maleimide-functionalized PEGylated DSPE (Mal-PEG-DSPE), combined at a molar ratio of 50:49:1, as previously described [35]. As control, a scrambled peptide sequence (H₂N-CKKKKLLSAVLWDELVDPLA-COOH) was coupled to the surface of cationic liposomes (Scr-lipo). Briefly, the lipids in chloroform were combined and dried in a rotary evaporator. Then, the lipid film was hydrated with molecular biology grade water to reach the final lipid concentration of 20 mM resulting multilamellar vesicles that were extruded through 100 nm polycarbonate membranes using a Mini-Extruder (Avanti Polar Lipids, Alabaster, AL/USA). Next, the P-selectin binding peptide was linked at the liposomes' surface by cysteine-maleimide reaction as previously described [38]. Finally, a purification step was performed to separate the liposomes from the uncoupled peptide, using the Amicon centrifugal filter units with a cut-off 100 kDa (Millipore). The amount of P-selectin binding peptide coupled at the surface of liposomes was indirectly determined by measuring the amount of uncoupled, free peptide collected from the filtrate, by high-performance liquid chromatography (HPLC) employing a UHPLC (Agilent 1290 Infinity, Agilent Technologies Santa Clara, California, USA), as previously described [34].

For in vitro uptake studies, the liposomes were fluorescently labeled by inserting the NBD-DSPE (1 mol%) into liposomes bilayers.

For biodistribution studies in mice, the phospholipid bilayers of liposomes were fluorescently labeled by adding Rhodamine B-PE (1 mol%) in the liposomes' composition.

Lipoplexes.

The targeted (Psel-lipo/shRNA) or non-targeted (Scr-lipo/shRNA) lipoplexes were obtained by complexation of the cationic liposomes with a mixture of the five MISSION®shRNA plasmids DNA targeting mouse RAGE gene (shRAGE) or with a control plasmid, MISSION® pLKO.1-puro Non-Mammalian shRNA Control Plasmid DNA (shCTR) at different charge ratios (R) +/-, 1:1 volume. The following five clones from The RNAi Consortium (TRC) Version 1 library containing shRNA sequences specific for mouse RAGE and cloned into the pLKO.1-puro vector were used: TRCN0000071743; TRCN0000071744; TRCN0000071745; TRCN0000071746; TRCN0000071747. The desired final quantities of cationic liposomes and shRNA plasmids were diluted in an equal volume of 150 mM NaCl, corresponding to about 10% of the final volume. The lipoplexes were formed by slowly pipetting the required volume of plasmids in a drop-by-drop manner in an equal volume of cationic liposomes and incubating for 30 min at room

temperature, while gently shaking. Finally, the lipoplexes were brought to the final working volume with 150 mM NaCl. The charge ratio was calculated considering that 1 nmol of cationic lipopolyamine DMAPAP corresponds to 3 nmols positive charges and 1 μ g DNA contains 3 nmols negative charges [39]. *Escherichia coli* host strain DH5 α was used to amplify the RAGE-shRNA plasmids that were subsequently isolated and purified using the GenElute-Plasmid Midiprep kit (Sigma-Aldrich, Germany), according to manufacturer's protocol.

2.3. Characterization of lipoplexes

Size and zeta potential.

The average hydrodynamic size of lipoplexes was determined by the dynamic light scattering (DLS) method employing the Zetasizer Nano ZS (ZEN 3600, Malvern Instruments, Malvern, UK). The Zeta (ζ) potential was determined by electrophoretic light scattering (ELS) using a Zeta dip cell (ZEN 1002) immersed into the sample. The measurements were performed at 25 °C using the Smoluchowski model. The results were analyzed using the Zetasizer Software 7.12 (Malvern Instruments, Malvern, UK).

Gel retardation assay.

The efficacy of shRNA plasmid complexation by cationic liposomes was investigated, at different charge ratios (+/-), by electrophoretic separation on 1% agarose gels stained with Midori Green, as previously described [40]. The samples were mixed with 6 \times Loading Buffer (0.05% Orange G, 30% glycerol), loaded into the gel, and the migration was performed using Tris-Acetate-EDTA buffer (40 mM Tris-HCl, 1% acetic acid, 1 mM EDTA) at 70 V for 20 min. The DNA bands were visualized using an UVP transilluminator.

Transmission electron microscopy.

For the morpho-structural characterization of the lipoplexes, a drop of lipoplex suspension was placed on a Formvar/carbon copper grid for 2 min, then the excess of liquid was removed and 1% uranyl acetate was dropped on the lipoplexes and allowed to dry for 1 min. The excess was removed with a filter paper and the grid was observed employing the STEM TALOS F200C Transmission Electron Microscope (TEM) operating at an acceleration voltage of 200 kV.

2.4. In vitro studies

2.4.1. Cell culture

The bEnd.3 cells, an immortalized murine endothelial cell line (EC) derived from brain endothelioma (European Collection of Authenticated Cell Cultures, cat no.96091929), were cultured in DMEM containing 10% FBS at 37 °C in a humidified 5% CO₂ incubator, according to the producer's recommendations.

THP-1 cells, a monocyte cell line (American Type Culture Collection, cat no. ATCC® TIB-202™), were grown in suspension in RPMI 1640 culture medium containing 5% inactivated FBS, at 37 °C, 5% CO₂ in an incubator. The cells were split up (1: 5) twice a week [41].

The cells were periodically checked for *Mycoplasma* contamination by PCR assay using specific primers for different *Mycoplasma species* and by a commercially available kit for bioluminescent assay (MycoAlert Mycoplasma Detection Kit from Lonza, Basel, Switzerland) and tested negative.

2.4.2. Evaluation of lipoplexes cytotoxicity

The XTT assay, which is based on the reduction of the tetrazolium salt of XTT (2,3-Bis-(2-methoxy-4-nitro-5-sulphophenyl)-2H-tetrazolium-5-carboxyanilide salt) to water-soluble orange-colored formazan compounds, proportional to the number of living, metabolic active cells, was used to evaluate the viability of bEnd.3 cells after exposure to lipoplexes. Briefly, bEnd.3 cells were seeded in 96-well culture plates and after 24 h the cells were either exposed to lipoplexes formed at various charge ratios (R = 4, 6, 8 and 10) with shRNA control plasmid (1 μ g shCTR/ ml) or stimulated with LPS (100 ng/ml LPS) for 24 h before exposure to

lipoplexes. The corresponding concentrations of liposomes used to obtain lipoplexes at different charge ratios were used as control. After 24, 48 and 72 h, the culture media was removed and replaced with XTT/PMS (phenazine methosulfate) solution (final concentration 0.2 mg/ml XTT, 5 μ M PMS) in colorless DMEM. After incubating for 2 h at 37 °C, the optical absorbance was measured at 450 nm using an Infinite® M200 PRO microplate reader (Tecan, Männedorf, Switzerland) spectrophotometer. The experiments were performed in triplicate and the results were expressed as percentage relative to untreated cells, considered control.

2.4.3. Uptake of P-selectin targeted lipoplexes by activated endothelial cells P-selectin expression on LPS-stimulated bEnd.3 cells.

The expression of P-selectin was determined, at 4 and 24 h, on the surface of non-activated or LPS-activated (100 ng/ml LPS) bEnd.3 cells, by flow cytometry using anti-human/mouse CD62P (P-selectin) PerCP-eFluor®710 (2 μ g/10⁵ cells) and a standard flow cytometry protocol using a Gallios Flow Cytometer (Beckman Coulter, Brea, CA, USA).

Lipoplexes uptake.

The cells were seeded in 24-well plates at a density of 25,000 cells/well. At 24 h after seeding, the cells were stimulated for 24 h with 100 ng/ml LPS to increase the surface expression of P-selectin. Then, the cells were incubated for 4 h at 37 °C with lipoplexes made of fluorescently labeled (NBD-DSPE) P-selectin targeted cationic liposomes (Psel-lipo) or non-targeted ones (Scr-lipo) and shCTR plasmid at charge ratio +/- of 6 (at a plasmid concentration of 0.6 μ g/ml). After that, the cells were harvested using 0.5 mM EDTA/ 0.25% trypsin and resuspended in FACS buffer consisting of 0.5% paraformaldehyde (PFA) in phosphate buffer saline (PBS) for flow cytometry determinations in the FL1 channel (530 nm), after excitation with the blue laser (488 nm) (Gallios, Beckman Coulter). Also, the uptake was visualized by fluorescence microscopy using the Olympus IX-81 microscope (Olympus America, Melville, NY).

2.4.4. RAGE expression on bEnd.3 endothelial cells

The expression of RAGE in bEnd.3 cells was analyzed by Western blot assay [42]. At 24 h after seeding in 6-well plates at a cell density of 2 \times 10⁵, the cells were stimulated for 4 and 24 h with 100 ng/ml LPS. Then, the cells were lysed with Sx2 Laemmli buffer (62.5 mM Tris pH 6.8, 20% glycerol, 2% SDS, Bromophenol blue, 0.25 M β -mercaptoethanol) and protein concentration was determined by Amido Black assay. Fifty μ g protein cell extracts were loaded on 12% SDS-PAGE and after electrophoretic separation (120 V, 60 mA), they were transferred onto nitrocellulose membranes using a Trans Blot Semi-Dry system (30 min at 15 V). The blots were blocked with 3% BSA/Tris-buffered saline with 0.1% Tween 20 (TBST) for one hour and incubated overnight (4 °C) with the primary antibodies: mouse anti-mouse RAGE (1:1000, Santa Cruz Biotechnology cat. no. sc-365,154) or mouse anti-GAPDH antibody (1:1000, Ambion cat. no. AM4300). After three washes of 10 min with TBST, the membranes were incubated with mouse IgG kappa binding protein (m-IgG κ BP) conjugated to Horseradish Peroxidase (HRP) (1:1000, Santa Cruz Biotechnology cat. no. sc-516,102) at room temperature for one hour. After washing in TBST, the blots were developed with SuperSignal™ West Dura Extended Duration Substrate (Thermo Fisher Scientific cat. no. 34076) and the detection of the protein bands was performed using the image reader LAS-4000 (General Electric, Healthcare, UK). The optical density (OD) of the protein bands was quantified using Image J (National Institutes of Health, Bethesda, MD, USA) and RAGE expression was normalized to that of GAPDH. The data were expressed as mean \pm S.D. (standard deviation) of two experiments performed in duplicates.

2.4.5. Transfection of bEnd.3 cells with Psel-lipo/shRAGE lipoplexes

The bEnd.3 cells were seeded in 6-well plates, at a cell density of 2 \times 10⁵ cells/well, and after 24 h were stimulated with LPS (100 ng/ml) for 24 h. Then, LPS-stimulated bEnd.3 cells were incubated with OptiMem

medium (Thermo Fisher Scientific cat. no. 31985062) containing non-targeted (Scr-lipo/shRAGE) or P-selectin targeted (Psel-lipo/shRAGE) lipoplexes, obtained as described above, at $R = 6$ (mix of five RAGE-shRNA plasmids at 1 μ g each, at a final concentration of 5 μ g/ml). As a negative control for RNA interference, lipoplexes formed with the MISSION® pLKO.1-puro non-mammalian shRNA control plasmid DNA (shCTR) with no homology to known mammalian genes was used. Also, other controls, namely the transfection with free shRAGE plasmids and non-transfected cells were used. The transfection medium was replaced after three hours with fresh DMEM supplemented with 10% fetal bovine serum and after 48 or 72 h, the cells were lysed and Western blot assay was performed as described above.

2.4.6. Monocyte adhesion assay

To investigate the functional role of down-regulating endothelial-RAGE in monocyte adhesion to endothelial cells, we performed the monocytes adhesion assay after treatment of LPS-activated bEnd.3 cells with lipoplexes carrying shRAGE. For this, bEnd.3 cells were cultured in 6-well plates and either activated for 24 h with LPS (100 ng/ml), or left unstimulated. Transfection was performed at a charge ratio $R = 6$ (final plasmid concentration of 5 μ g/ml) with lipoplexes Psel-lipo/shRAGE, Scr-lipo/shRAGE, Psel-lipo/shCTR or with free shRAGE. After 72 h, THP-1 monocytes, fluorescently labeled with BCE-CF (2',7'-bis-(2-carboxyethyl)-5-(and-6)-carboxy fluorescein), were co-incubated (at a ratio of 1:2) with LPS-activated or resting endothelial cells for 30 min, at 37 °C. Non-adherent monocytes were removed by washing with RPMI medium, and the monocytes that adhered to the endothelial cells were counted on six different microscope fields per sample with an inverted fluorescence microscope (IX-81, Olympus America, Melville, NY), using the FITC filter. Images were acquired with CellSense Dimensions software.

2.5. Animal studies

Male ApoE-deficient mice (B6.129P2-Apo^{tm1Unc}/J; Stock No: 002052) from The Jackson Laboratory were housed in individually ventilated cages in a specific pathogen-free facility on a 12-h light/dark cycle, with unrestricted access to food and fresh water. To accelerate the progression of atherosclerotic lesions, the animals were placed on a high-fat diet (HFD) consisting of standard chow rodent diet with 15% butter (82% fat) and 1% cholesterol. Throughout the experiments, the weight of the animals was monitored, as a welfare parameter.

The study protocols and experiments were approved by the Ethics Committee of the Institute of Cellular Biology and Pathology "Nicolae Simionescu" and by the National Sanitary Veterinary and Food Safety Authority authorization no. 295/23.08.2016 and were performed in accordance with the Romanian Law no. 43/2014 (Official Monitor, Part I nr. 326: p 2–4), which transposes the EU directive 2010/63/EU on the protection of animals used for scientific purposes.

2.5.1. Biodistribution of P-selectin targeted lipoplexes

Six-month old ApoE-deficient mice (20–25 g of weight) had been on HFD for other four-weeks before the i.v. injection of the fluorescently-labeled lipoplexes. The P-selectin targeted or non-targeted PEGylated cationic liposomes were labeled with Rhodamine B-DSPE (1 mol%) and the lipoplexes made with the shRNA Control plasmid (shCTR) were administered retro-orbitally, under anesthesia, at a dose of 10 μ mol lipids/1.5 mg shCTR ($R = 6$) per kg body weight (150 μ l/mouse) ($n = 3$ for each lipoplexes formulation). As control for autofluorescence, a mouse which received 0.9% saline solution was investigated. After one hour, the mice were anesthetized with ketamine/xylazine, exsanguinated via open heart puncture and the vasculature was rinsed using a peristaltic pump (infusion rate 2.5 ml/min) with cold PBS containing 5 mM EDTA while the right atrium was punctured to allow removal of the systemic blood. The organs (lungs, heart, aorta, liver, spleen, kidneys, and the brain) were excised and their fluorescence was visualized with

an IVIS Imaging System 200 (Caliper Life Sciences), using $\lambda_{ex} = 535$ nm and $\lambda_{em} = 580$ for Rhodamine B. For spectral unmixing and discrimination between Rhodamine B fluorescence and tissue autofluorescence, several emission wavelengths were used (580 nm, 600 nm, 620 nm, 640 nm, and 660 nm).

2.5.2. Transfection efficiency of P-selectin targeted lipoplexes in ApoE-deficient mice

To evaluate the ability of P-selectin-targeted lipoplexes to function as effective vectors for shRNA plasmids delivery to the inflamed vasculature of ApoE-deficient mice, the lipoplexes were formed by complexation of a plasmid encoding the green/yellow fluorescent protein derived from *Aequorea Victoria* (pEYFP) with cationic liposomes directed or not to P-selectin. ApoE-deficient mice received a single dose retro-orbital injection of Psel-lipo/pEYFP or Scr-lipo/pEYFP lipoplexes ($R = 6$) containing 1.5 mg plasmid DNA/kg body weight in a volume of 150 μ l/mouse. After 48 h, the mice were anesthetized and the vasculature was washed with PBS containing 5 mM EDTA. The organs (heart, lung, liver, kidney, spleen, brain) were collected and trimmed to remove peripheral fatty tissue, and were visualized with an IVIS Imaging System 200 (Caliper Life Sciences) using the excitation and emission wavelengths for the YFP protein of $\lambda_{ex} = 500$ nm and $\lambda_{em} = 540$ nm. For spectral unmixing and discrimination between YFP protein fluorescence and tissue autofluorescence, several λ_{em} were used (540 nm, 560 nm and 580 nm).

2.5.3. Investigation of RAGE downregulation after administration of Psel-lipo/shRAGE lipoplexes

For the RAGE downregulation study, six-month old, male ApoE-deficient mice ($n = 9$ mice/experimental group) were injected twice a week for four weeks with lipoplexes carrying shRAGE plasmids (1.5 mg plasmid DNA/kg body weight, 150 μ l/mouse) either targeted (Psel-lipo/shRAGE) or non-targeted (Scr-lipo/shRAGE) and simultaneously fed with the HFD. As controls, the administration of P-selectin targeted lipoplexes containing shCTR and PBS were used. No mice died in any experimental group. Four days after the last injection, the blood was collected in EDTA-tubes by cardiac puncture and then, the vasculature was rinsed with cold PBS using a peristaltic pump (infusion rate 2.5 ml/min). The organs and aorta (from the left ventricle to the iliac bifurcation) were collected, the fat tissue trimmed away, then the organs were snap frozen in liquid nitrogen and stored at -80 °C until tissue homogenization. For Western blot analysis, the tissue samples were homogenized in Laemmli 2 \times buffer (Merck, cat no. S3401) using a Silent Crusher M homogenizer from Heidolph, sonicated for 15 s and denatured by boiling for 10 min. Protein concentration was determined by Amido black assay and the RAGE protein expression was investigated by Western blot as above described.

Also, the aortic roots, collected by cutting the hearts transversally below the atriums, were fixed in 4% PFA/PBS overnight, then cryoprotected with glycerol and maintained at -20 °C until embedded in Optimal Cutting Temperature (OCT) compound. Lung, liver, and kidney pieces were fixed in formalin and embedded in paraffin for histology investigations.

2.5.4. Assessment of the anti-inflammatory effect of Psel-lipo/shRAGE lipoplexes administration

The expression of inflammatory molecules in the aorta of ApoE-deficient mice after the treatment with lipoplexes was investigated by Western blot analysis. The tissue samples were homogenized by sonication in Sx2 Laemmli buffer and 40 μ g total protein were loaded per lane on 5–20% gradient SDS-PAGE gel. The proteins were electrophoretic separated and then transferred onto nitrocellulose membranes using a Trans Blot Semi-Dry system (15 V/15 min/gel). After being blocked with 3% BSA/TBST, the blots were incubated overnight with the primary antibodies: anti-NF- κ B p65 (1:1000, Abcam, cat no. ab16502), anti-TNF- α (1:1000, Santa Cruz, cat no. sc8301) and anti-beta tubulin

antibody (1:1000, Abcam, cat. no. ab6046) as loading control. Then, after washing, the membranes were incubated with HRP-conjugated goat anti-rabbit IgG (H + L) secondary antibody (1:1000, Invitrogen, 32,460) for one hour at room temperature. The blots were developed with SuperSignal™ West Dura Extended Duration Substrate (Pierce) and the bands were detected with an image reader LAS-4000. The optical density (OD) of the protein bands was quantified using Image J and the expression of NF- κ B and TNF- α was normalized to that of beta-tubulin.

2.5.5. Determination of plasma inflammatory cytokines

The pro-inflammatory cytokines IL-1 β , IL-6, TNF- α , and the chemokine MCP-1, were quantified using ELISA DuoSet kits (R&D systems, Minneapolis, MN, USA cat. no. DY401, DY406, DY410 and DY479 respectively), following the manufacturer's instructions. Briefly, the plasma (diluted 1:10 in PBS) was incubated for two hours at room temperature (RT) in 96-well plates covered with the capture antibody specific for the investigated molecule, as indicated by the manufacturer. After washing with the provided buffer, the detection antibody was added (2 h, RT), followed by Streptavidin-HRP and the detection of the optical density using an Infinite® M200 PRO microplate reader (Tecan, Männedorf, Switzerland) spectrophotometer. The concentration of IL-1 β , IL-6, TNF- α and MCP-1 were calculated after plotting their corresponding standard curves.

2.5.6. Immunofluorescence and tissue histology

Tissue processing.

Explanted specimens of the aortic roots were embedded in OCT compound for cryosectioning. The sections of the aortic roots were harvested when the first valve cup became visible in the lumen of the aorta. Five μ m thick sections were harvested and placed on a microscope slide (4 sections/slide), and 10 slides were prepared per mouse.

Immunofluorescence.

To reveal RAGE and NF- κ B expression in the aortic roots, heat-induced epitope retrieval (HIER) was performed. The cryosections were rinsed three times in PBS and then incubated in Tris buffer (50 mM Tris HCl, Sigma-Aldrich T3253, pH 9.0) at 97 °C for 3 h. After cooling at room temperature for one hour, the slides were rinsed in PBS and incubated over night at 4 °C with the primary antibody (RAGE A-9, Santa Cruz Biotechnology, cat no. sc-365,154, or NF- κ B p65, Abcam, cat no. ab16502) diluted 1:100 in 1% BSA/PBS. The next day, the slides were incubated with the appropriate secondary antibody (Alexa Fluor 594 chicken anti-mouse, Invitrogen, cat no. A21201, and Alexa Fluor 594 donkey anti-rabbit, Invitrogen, cat no. A21207, respectively) diluted 1:1000 in 1% BSA/PBS. After rinsing, the slides were mounted with ProLong Gold Antifade Mountant with DAPI (ThermoFisher-Scientific, P36931). Fluorescence micrographs were captured using XM10 camera attached to a Olympus IX81 inverted microscope (IX81-ZDC) and the cellSens Dimension software (Olympus), using the same acquisition settings throughout the experiment. Image processing was performed using Fiji Is Just ImageJ (NIH) freeware, with the same protocol between samples. Images acquired with 20 \times and 40 \times magnification were stitched together with the Stitching (Linear blending) plug-in in order to obtain whole detailed images.

Lipid staining with Oil Red O in the aortic root.

The aortic root was stained for the neutral lipid content of the atherosclerotic lesions using the Oil Red O (ORO) staining assay [43]. Aortic root cryosections were rinsed 30 min with PBS and incubated in 0.3% ORO (Sigma-Aldrich, O0625) diluted in 60% isopropanol for 15 min. After brief rinsing in PBS, the slides were immersed in 60% isopropanol for five minutes and rinsed again in PBS. The nuclei were counterstained by incubating with hematoxylin (Hematoxylin and Eosin stain kit, VECTOR Laboratories, H-3502) for 3 min. After rinsing with distilled water, the slides were mounted with coverslips using 90% glycerol. The images were taken using a camera equipped Leica DMi1 inverted light microscope. The lesion area was quantified morphometrically employing ImageJ freeware for measurement of the lesion area of

the aortic root in 10 sections per mice. The percentage of area occupied by lesions was calculated by dividing the surface of the lesions by the surface of total aortic root as previously described [43].

2.5.7. Safety evaluation of P-sel/shRAGE lipoplexes

Biochemical blood parameters.

Blood was collected from mice from different experimental groups in EDTA-tubes and the plasma was obtained by centrifugation at 2000 rpm for 20 min at room temperature, and stored at -80°C until performing the assays. The biochemical measurements were performed using Dia-Lab reagent kits for cholesterol (cat no. D95116), triglycerides (cat no. D00389), plasma urea (BUN; cat no. 402999), creatinine (cat no. D95595), transaminases aspartate aminotransferase (AST; cat no. D94610), alanine aminotransferase (ALT; cat no. D94620), alkaline phosphatase (ALP; cat no. D95564), according to manufacturer's instructions. Briefly, volumes of each sample were pipetted into 96-well plates and the appropriate volumes of reagents were added. Immediately, in the case of enzymatic assays, or after the indicated incubation time, the absorbance was measured using an Infinite® M200 PRO microplate reader (Tecan, Männedorf, Switzerland) spectrophotometer at the recommended wavelength. The concentration of the parameters was determined by the simultaneous measurements of the recommended standards (Assayed Universal Calibration Serum; cat no. D98485, Dical Autor).

Histopathological analysis of lungs, liver and kidneys of mice injected with Psel-lipo/shRAGE.

Lung, liver and kidney pieces were fixed in formalin and embedded in paraffin. The $5\ \mu\text{m}$ -thick paraffin sections were stained with hematoxylin and eosin (H&E) stain kit (VECTOR Laboratories, cat. no. H-3502), according to the manufacturer's guide. The light micrographs were taken using a Leica DMi1 inverted microscope equipped with a camera. In lung sections, the alveolar septal wall thickness and the number of nuclei, as a measure of cellular density, were quantified by analyzing optical microscopy micrographs taken with $20\times$ objective using ImageJ 1.53c freeware (NIH, USA) according to the macro described in the Supplementary material. Ten random fields were used per mouse.

In vitro hemocompatibility assays.

The hemocompatibility of Psel-lipo/shCTR lipoplexes was investigated by determining the hemolysis and erythrocyte aggregation induced by their incubation in the presence of lipoplexes. Blood samples were collected in EDTA tubes by cardiac puncture from C57BL/6 J mice (12-week-old male; Stock No: 000664, The Jackson Laboratory), and the hemolysis assay was performed as previously described [44]. Briefly, isolated erythrocytes were diluted 1:10 in PBS (pH 7.4) containing Psel-lipo/shCTR lipoplexes at different charge ratios ($R = 4, 6, 8$ and 10) and further incubated at 37°C , for 1 h. The concentration of shRNA plasmid was calculated to imitate the in vivo conditions of i.v. administration, in which lipoplexes containing $30\ \mu\text{g}$ plasmid DNA was injected into a mouse (having approximately 1 ml of blood, 45% erythrocytes). Then, the samples were centrifuged to sediment the intact erythrocytes, and the hemoglobin released in the supernatants was measured with a plate reader (TECAN Infinite M200Pro) at 540 nm. As negative and positive controls, the incubation of erythrocytes in PBS and in 0.5% Triton X-100 (considered 100% hemolysis), respectively, were used. The percentage of lysed erythrocytes was calculated using the formula:

$$\% \text{Hemolysis} = 100 \times \frac{A_{\text{sample}} - A_{\text{negative control}}}{A_{\text{positive control}} - A_{\text{negative control}}}$$

where A is the absorbance at 540 nm.

To study the aggregation of erythrocytes induced by lipoplexes, pelleted erythrocytes were resuspended in PBS, placed on glass slides and examined with an Olympus IX81 light microscope.

2.6. Statistical analysis

The results are expressed as mean \pm standard deviation (SD). Statistical analyses were carried out using GraphPad Prism 7 software (GraphPad Software, La Jolla, CA) and statistical differences were evaluated with unpaired two-tailed *t*-test for the comparison of two groups or one-way ANOVA with multiple comparisons post-hoc Tukey test for comparison of three or more groups. Statistically significance of differences: * $p < 0.05$, ** $p < 0.01$, *** $p < 0.001$.

3. Results and discussion

3.1. Characterization of lipoplexes

Based on previous experience, we developed P-selectin targeted PEGylated cationic liposomes (Psel-lipo) [35] to act as non-viral vectors for shRNA plasmids delivery intended to interfere with RAGE transcription. Psel-lipo were prepared using the extrusion method of hydrated lipid mixture comprising DMAPAP (cationic lipid), DOPE (helper lipid), and maleimide-functionalized phospholipidic derivatives of PEG (Mal-PEG-DSPE) used for coupling the peptide with affinity for P-selectin at the liposome's surface. As a control, PEGylated cationic liposomes coupled with a scrambled peptide (Scr-lipo) were prepared. The HPLC measurements determined an amount of about $9.5\ \mu\text{g}$ peptide per μmol lipid coupled to the surface of liposomes, as elsewhere reported [35].

To evaluate the degree of shRNA plasmid complexation by Psel-lipo, the electrostatic lipoplexes of Psel-lipo with shRNA control plasmid (Psel-lipo/shCTR), formed at different charge ratios (R) $+/-$ (0.25, 2, 4, 6, 8 and 10), were loaded into the agarose gel containing Midori-Green. The shCTR plasmid lanes were visualized under UV light (Fig. 1A). Compared to free shCTR, the migration of shCTR plasmid is completely blocked for Psel-lipo/shCTR lipoplexes obtained at $R \geq 4$, indicating that starting with $R = 4$, the shRNA plasmid is efficiently covered by the PEGylated cationic liposomes (Fig. 1A).

The images obtained by negative staining transmission electron microscopy (TEM) revealed the condensed multilamellar structures appearance ("fingerprint-like") of lipoplexes with concentric lamellar structures formed by alternating lipid bilayers of liposomes and plasmid DNA (Fig. 1C). Concentric lamellar structures form vesicles with diameters of $\sim 100\ \text{nm}$ (mean size of $102 \pm 9\ \text{nm}$).

Size and ζ -potential measurements of the liposomes and corresponding lipoplexes are summarized in Fig. 1B. Dynamic light scattering analysis (DLS) indicated that, immediately after preparation, the average hydrodynamic diameter of lipoplexes Psel-lipo/shCTR and Scr-lipo/shCTR obtained at $R = 6$ was around $150\ \text{nm}$ and had a unimodal distribution, as shown by the polydispersity index (PDI), which was below or around 0.2 (Fig. 1B). There were no significant differences in the liposomes and lipoplexes with respect to size characteristics immediately after preparation. The higher size obtained by DLS measurements in comparison with TEM determinations can be explained by the fact that DLS measurements were done using intensity distribution mode and provide the mean hydrodynamic diameter of solvated nanoparticles in solution, whereas in TEM the samples are investigated in the dry state [45].

The ζ -potential of liposomes had a positive value of $\sim +35\ \text{mV}$ for both Psel-lipo and Scr-lipo. The interaction between shRNA plasmid and cationic liposomes produced a decrease of the ζ -potential to $\sim +20\ \text{mV}$, indicating the electrostatic attraction between the cationic liposomes and the negatively charged shRNA plasmid during the lipoplexes formation.

To check the stability of the lipoplexes, we have periodically assessed their size after different time intervals (for up to 4 weeks) of storage at 4°C . Representative results of one set of measurements performed on liposomes and lipoplexes ($n = 4$) are summarized in Supplementary Table S1. Since no significant deviation in dimensions after the 4-week

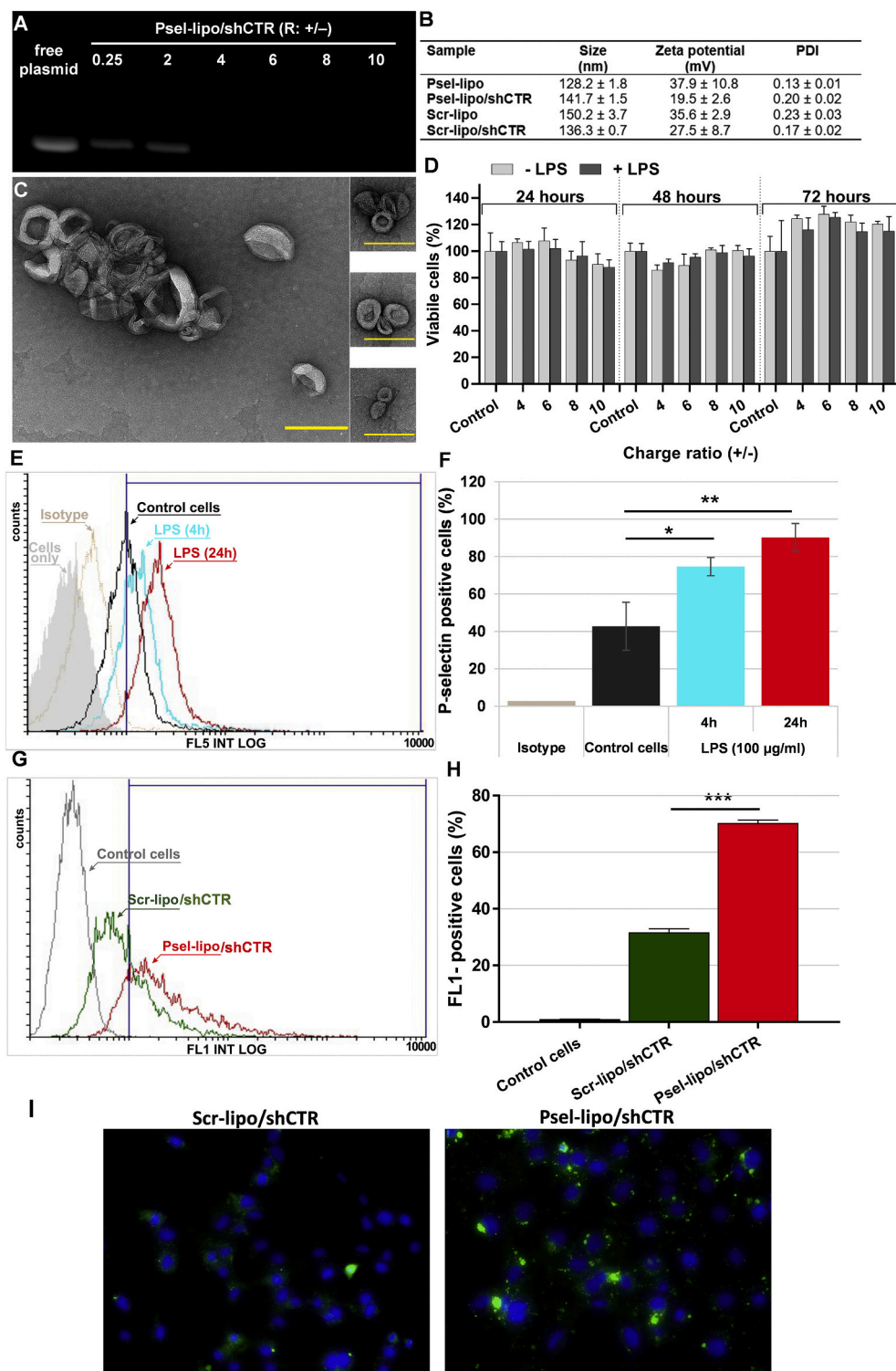


Fig. 1. Characterization of P-selectin targeted lipoplexes. (A) Agarose gel retardation assay performed for free shRNA plasmid (shCTR) and Psel-lipo/shCTR lipoplexes at different charge ratios \pm (R) (200 ng shCTR/lane). (B) Average hydrodynamic diameter and ζ -potential of P-selectin targeted liposomes (Psel-lipo) and lipoplexes (Psel-lipo/shCTR) and non-targeted liposomes (Scr-lipo) and lipoplexes (Scr-lipo/shCTR) at R = 6 for 100 nM final shCTR concentration. Results are reported as mean \pm SD for five individual measurements. (C) Electron micrographs of negatively-stained Psel-lipo/shCTR lipoplexes (R = 6). Scale-bars: 200 nm. (D) Viability of quiescent endothelial cells (EC, bEnd.3 cell line) or LPS-activated EC, incubated for different periods (24, 48 and 72 h) with Psel-lipo/shCTR lipoplexes at various ratios (4, 6, 8 and 10) (1 μ g shRNA/ml). The results were normalized to untreated (control) cells. Data are presented as mean \pm SD of a representative experiment made in three replicates. (E) Overlay of representative flow cytometry histograms showing the expression of P-selectin on the surface of quiescent (untreated, black line) and of LPS (100 ng/ml)-treated EC for 4 or 24 h (cyan and red lines, respectively). (F) Percentages of P-selectin positive cells as determined by flow cytometry experiments and plotted from a single experiment using triplicate probes. Bar graph shows data as mean \pm SD. Statistical significance: * $p < 0.05$, ** $p < 0.01$. (G) Overlay of representative flow cytometry histograms demonstrating uptake of fluorescently-labeled Psel-lipo/shCTR and Scr-lipo/shCTR lipoplexes after 4 h of incubation with LPS-activated EC. (H) Comparison between the uptake of P-selectin targeted (Psel-lipo/shCTR) and non-targeted (Scr-lipo/shCTR) lipoplexes by EC, expressed as percentage of FL1-positive cells. Data are mean \pm SD of a representative experiment performed in triplicate. (I) Fluorescence images of LPS-activated EC incubated with fluorescently labeled Scr-lipo/shCTR and Psel-lipo/shCTR lipoplexes (green). Nuclei are stained with DAPI (blue). Scale bar: 20 μ m. (For interpretation of the references to colour in this figure legend, the reader is referred to the web version of this article.)

storage period was observed, except for an increase in the PDI at the end of the period (0.32 ± 0.05), we may assume that the lipoplexes can be used within one month without significant alterations of their size. However, in the experiments, we used the lipoplexes immediately after preparation.

3.2. Effect of P-selectin targeted lipoplexes on endothelial cells: In vitro studies

3.2.1. Lipoplexes are not cytotoxic for endothelial cells

Potential cytotoxicity induced by the exposure of quiescent and LPS-activated EC (bEnd.3 cell line) to Psel-lipo/shCTR lipoplexes for different intervals (24, 48 and 72 h) was assessed using XTT assay. The data showed that the viability of quiescent and LPS-activated bEnd.3 cells was not significantly affected by the incubation with P-selectin

targeted lipoplexes (Fig. 1D) or non-targeted ones (Supplementary Fig. S1) formed with the shRNA control plasmid (1 µg shCTR/ ml) at various charge ratios $R = 4, 6, 8$ and 10 . The data show that lipoplexes are cyto-compatible and can be further used in transfection experiments.

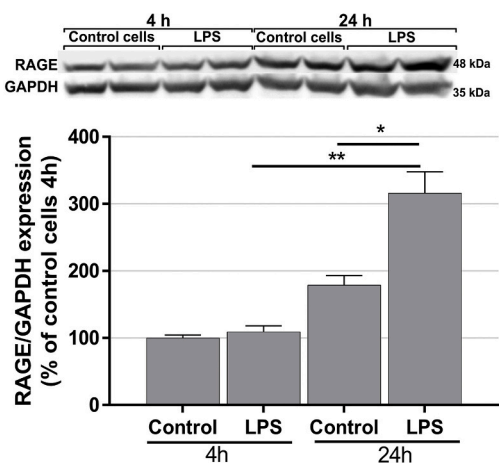
3.2.2. P-selectin targeted lipoplexes are taken up by endothelial cells

3.2.2.1. P-selectin is over-expressed on the surface of LPS-activated cultured EC. The expression of P-selectin on the surface of quiescent or LPS-activated EC was assessed by flow cytometry. In the absence of LPS activation, ~ 40% of EC express P-selectin (Fig. 1E and F). The activation of EC with LPS (100 ng/ml) for 4 and 24 h induced a significant increase, of about two-fold, in P-selectin expression. When the EC were

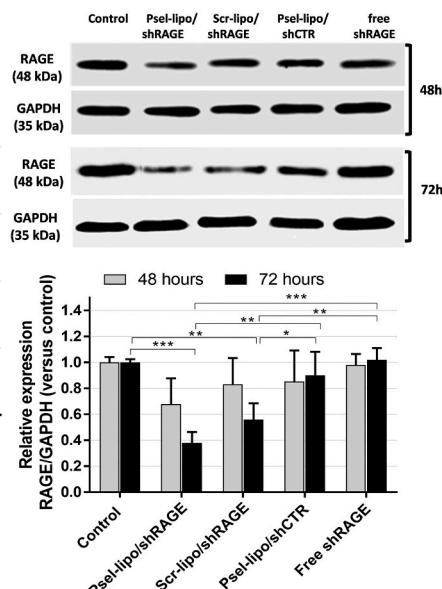
exposed for 24 h to LPS, it was found that ~90% of the cells were positive for P-selectin. For this reason, in all subsequent studies, the cells were activated for 24 h with 100 g/ml LPS and then used to assess the interaction of P-selectin targeted and non-targeted lipoplexes with the endothelial cells.

3.2.2.2. P-selectin targeted lipoplexes are efficiently taken up by LPS-activated endothelial cells. For efficiently silencing the target gene, the shRNA plasmid has to be intracellularly delivered into the cells. To this purpose, the uptake of fluorescently-labeled Psel-lipo/shCTR and Scr-lipo/shCTR lipoplexes ($R = 6$; $0.6 \mu\text{g shCTR/ml}$) by the LPS-activated EC was investigated after a 4-h incubation at 37°C by flow cytometry. As shown in Fig. 1G and H, a 2.3-fold increase in the percentage of cells

A: RAGE expression in bEnd.3 cells



B: RAGE downregulation by lipoplexes



C: Monocyte adhesion to LPS-activated bEnd.3 cells treated with lipoplexes

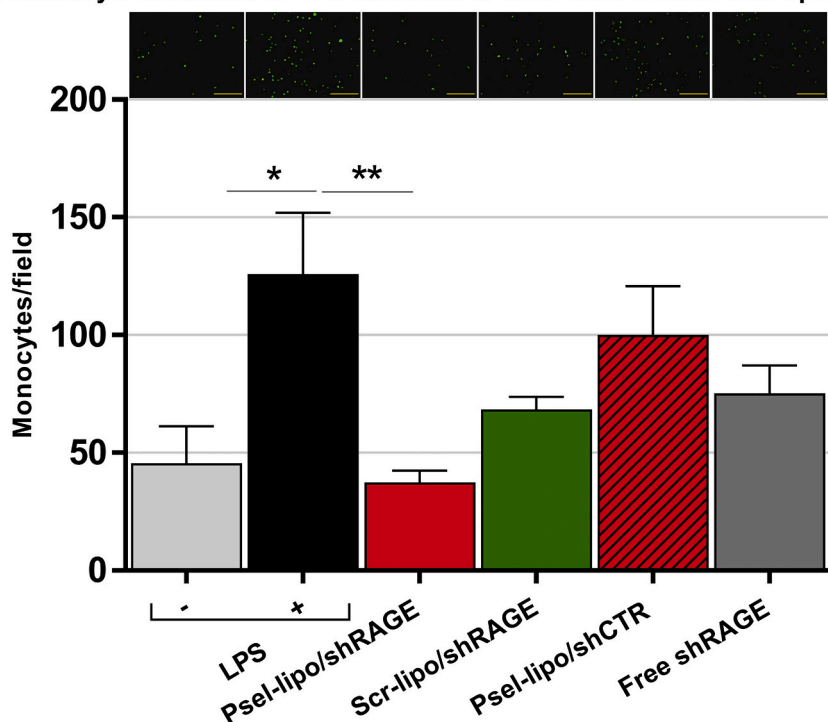


Fig. 2. (A) RAGE protein expression in quiescent and LPS-activated endothelial cells (EC, bEnd.3 cell line) for 4 and 24 h. The data of Western blot experiments expressed as mean \pm SD, are representative of three independent experiments performed in duplicates. (B) Representative Western blot and densitometric analysis of RAGE protein expression in LPS-activated EC treated with Psel-lipo/shRAGE, Scr-lipo/shRAGE, Psel-lipo/shCTR lipoplexes and free shRAGE, normalized to control, untreated cells, at 48 and 72 h. The histogram depicts data from three independent experiments expressed as mean \pm SD. (C) Functionality of different type of lipoplexes in the reduction of monocytes adhesion to LPS-activated EC compared with free shRAGE. Representative fluorescence micrographs show the adherent fluorescently-labeled monocytes (green) to activated EC treated with Psel-lipo/shRAGE, Scr-lipo/shRAGE, Psel-lipo/shCTR lipoplexes and free shRAGE. Scale bar: 200 µm. The histogram presents the results as mean \pm SD of three experiments performed in duplicates. Statistical significance: * $p < 0.05$, ** $p < 0.01$, *** $p < 0.001$. (For interpretation of the references to colour in this figure legend, the reader is referred to the web version of this article.)

detected in the FL1 channel, corresponding to the fluorescence of NBD-DSPE inserted into the liposomes' bilayers, was detected in the case of EC incubation with Psel-lipo/shRNA as compared to Scr-lipo/shRNA lipoplexes, demonstrating a higher internalization of P-selectin targeted lipoplexes. In addition, the fluorescence images showed small green fluorescent granules inside the cytosol, indicating the internalization of lipoplexes (Fig. 1I). It can be observed that, in the case of incubation with Psel-lipo/shCTR, the cells displayed more numerous fluorescence dots, suggesting a higher cellular internalization of P-selectin targeted lipoplexes than non-targeted ones. These data are in good agreement with our previous study that showed a higher uptake, in both static and dynamic conditions of incubation, of lipoplexes made of cationic Psel-lipo and siRNA in comparison with control, cationic liposomes coupled with a scrambled peptide (Scr-lipo/siRNA) [35]. In the same study, competitive experiments, performed in the presence of an excess of P-selectin binding peptide, demonstrated that targeted lipoplexes are specifically internalized by a P-selectin mediated mechanism.

It has been reported that physicochemical properties of lipoplexes, such as size, lipid/DNA charge ratio, the chemical structure of the lipids, and the presence of electrolytes, influence the intracellular delivery, and as a consequence, the transfection efficiency [27,46]. On the other hand, different cell types have a different rate of uptake and ability to express the sequence coded in a plasmid DNA, and therefore, it is difficult to predict the structure or lipoplex size that is most appropriate for the DNA/RNA delivery. The advantage of our approach is the targeting of an internalizing cell adhesion molecule that improves the delivery efficiency by increasing the cellular uptake of lipoplexes.

3.2.3. Transfection with Psel-lipo/shRAGE lipoplexes down-regulates RAGE expression in endothelial cells

3.2.3.1. RAGE expression in bEnd.3 cells. RAGE protein expression level in bEnd.3 cells, cultured in normal- or exposed to LPS conditions was evaluated by immunoblotting. We found that RAGE protein was constitutively expressed by quiescent bEnd.3 cells, in line with previous reports [47]. The activation of cells with 100 ng/ml LPS for 24 h up-regulated its expression by ~ twofold as compared to non-activated cells (Fig. 2A).

3.2.3.2. Psel-lipo/shRAGE lipoplexes significantly reduce RAGE at 72 h after transfection. Two types of lipoplexes, either P-selectin targeted (Psel-lipo/shRAGE) or non-targeted (Scr-lipo/shRAGE), were used to deliver into the EC, the mix of the five shRNA plasmids ($R = 6, 5 \mu\text{g/ml}$) containing sequences that specifically target RAGE mRNA or a shRNA control plasmid containing scrambled-shRNA sequence (shCTR). In Fig. 2B, RAGE protein levels relative to glyceraldehyde-3-phosphate dehydrogenase (GAPDH) are presented as fold change compared to the control, non-transfected cells. As one can see, the protein expression level of RAGE was significantly reduced in the cells treated with both types of lipoplexes carrying the shRNA plasmids targeting RAGE mRNA at 72 h after the EC transfection. Thus, Psel-lipo/shRAGE lipoplexes downregulated the expression of RAGE by 62% ($p < 0.001$), whereas the RAGE protein level was reduced by 44% ($p < 0.01$) when the transfection was performed using Scr-lipo/shRAGE lipoplexes. However, there was no statistically significant difference between targeted and non-targeted lipoplexes. This result could be explained by the fact that, although the uptake of Psel-lipo/shRNA lipoplexes was twofold higher than that of Scr-lipo/shRNA lipoplexes in the first 4 h of incubation, the level of RAGE-shRNA delivered intracellularly was sufficient to obtain a similar reduction of RAGE protein expression after 72 h. The data are in line with our previous results [35] and with those reported by Ásgeirsdóttir et al. [48] showing no difference for VE-cadherin silencing in activated glomerular endothelium between E-selectin targeted and non-targeted transfection using liposomes incorporating high doses of

siRNA (60 nM).

A statistically significant reduction was attained when RAGE protein expression, measured after transfection with Psel-lipo/shRAGE or Scr-lipo/shRAGE lipoplexes, was compared with its expression in cells transfected with Psel-lipo/shCTR or free shRAGE plasmids. These results demonstrated that the lipoplexes carrying shRNA sequences for RAGE silencing were effective in RNA interference, producing a significant downregulation of RAGE protein expression with a higher percent of reduction for P-selectin targeted lipoplexes.

3.2.4. Psel-lipo/shRAGE lipoplexes decrease the monocyte adhesion to LPS-activated endothelial cells

The involvement of RAGE in the inflammatory activation of endothelial cells has been well documented. It was previously demonstrated that the interaction of RAGE with its ligand S100B increases the activation of the ERK and JNK MAPKs pathways and the expression of cell adhesion molecules (e.g. VCAM-1) in murine and human aortic endothelial cells [4]. In human umbilical vein endothelial cells (HUVEC), RAGE expression is increased under shear stress conditions [49] and RAGE activation by HMGB1 induces the NF- κ B activation and increases the expression of TNF- α [50]. Besides, endothelial RAGE function as an adhesion receptor recognized by the integrin Mac-1 expressed on leukocytes, promoting thus leukocyte recruitment at the inflammatory sites of the vascular wall [8,9]. RAGE is involved in both the recruitment and activation of the inflammatory cells, thus playing an important role in the initiation and maintenance of inflammation [9,51]. To validate the role of RAGE in the increased adhesion of monocytes to the endothelial cells' monolayer, we transfected LPS-activated EC with Psel-lipo/shRAGE and Scr-lipo/shRAGE lipoplexes. The cells were first incubated with LPS (for 24 h) followed by incubation with Psel-lipo/shRAGE, Scr-lipo/shRAGE or Psel-lipo/shCTR lipoplexes and free shRAGE (for 72 h). After incubation of EC with fluorescently labeled monocytes (for 30 min), the non-adhered monocytes were removed by thorough washing, and the fluorescently adherent monocytes were counted. As shown in Fig. 2C, the activation of EC with LPS caused a considerable increase (~3-fold) in monocyte adhesion compared to monocyte adhesion to unstimulated, control cells. Transfection of LPS-activated EC with Psel-lipo/shRAGE significantly reduced the number of adhered monocytes (~70%) compared to LPS-activated cells, while transfection with Scr-lipo/shRAGE decreased the monocytes adhesion by ~45%. Incubation of LPS-activated EC with Psel-lipo/shCTR lipoplexes and free shRAGE had no considerable effect on the monocyte adhesion process. Functionally, the higher percent of inhibition of monocytes adhesion to activated EC treated with Psel-lipo/shRAGE, as compared with the same concentration of shRAGE plasmid mix delivered by Scr-lipo/shRAGE (Fig. 2C), is a reliable indicative of RAGE role of in the monocyte adhesion to activated EC and the superior anti-inflammatory effect of Psel-lipo/shRAGE.

3.3. Effect of P-selectin targeted lipoplexes on experimental atherosclerosis: Animal studies

3.3.1. Biodistribution of P-selectin targeted lipoplexes after i.v. administration in ApoE-deficient mice

It was shown that P-selectin is a cell adhesion molecule with a key role in the progression of atherosclerotic lesions, mediating leukocyte recruitment into atheroma in ApoE-deficient mice [52]. Importantly, the expression of P-selectin is increased on the endothelium covering human atherosclerotic plaques [53] and in the aorta of hypercholesterolemic rabbits [54]. Also, P-selectin mRNA expression in the aorta of ApoE-deficient mice is strongly correlated with the progression of lesion formation, suggesting that P-selectin is a good targeted candidate for intervention, lesion imaging, or therapeutic targeting strategies [37,55]. Moreover, P-selectin has been reported as a reliable target for atherosclerotic plaque imaging in ApoE-deficient mice using magnetic resonance imaging (MRI) [56,57] and positron emission tomography (PET)

[58]. Apart from atherosclerosis, P-selectin was also investigated in preclinical and clinical studies as an imaging biomarker of other inflammatory conditions, such as thrombus, aneurysm, or ischemic stroke [59,60] or as a therapeutic target for sickle cell disease and myocardial infarction using the antibodies crizanlizumab and inclacumab, respectively [61,62]. Moreover, P-selectin was exploited as a target for nanocarriers-based delivery of therapeutic agents to inflammatory sites [34] and various tumors [63,64].

Therefore, our approach to use P-selectin as a molecular target for delivering lipoplexes to atherosclerotic lesions is justified by the previously accumulated data. Thus, we investigated whether the biodistribution of P-selectin targeted lipoplexes is different from that of non-targeted lipoplexes. The Rhodamine B-labeled Psel-lipo/shCTR or Scr-lipo/shCTR lipoplexes (1.5 mg of plasmid/kg body weight) were administered to ApoE-deficient mice by retro-orbital injection. After one hour, the mice's vasculature was washed with PBS by puncture of the left ventricle, and several organs (brain, lungs, heart, liver, spleen, kidneys) and aortas were removed and visualized ex-vivo using the IVIS Caliper 200 imaging system. The fluorescent radiant efficiency [fluorescence emission radiance per incident excitation intensity (p/s/cm²/sr)/(μW/cm²)] measurements using region-of-interest (ROI) function of Living Image 4.3.1. software was used to quantify the biodistribution of lipoplexes. The autofluorescence of organs isolated from mice injected with PBS only was subtracted from the ROI values measured for each organ. To delineate between tissue autofluorescence and the specific fluorescence of Rhodamine B, spectral unmixing was performed.

The fluorescence emission results show that, at one hour after administration, both types of lipoplexes accumulate mainly in the lungs and the liver of the mice (Fig. 3A-a, b). The non-targeted Scr-lipo/shCTR lipoplexes displayed increased accumulation in the lungs and the liver (Fig. 3A-b) compared to Psel-lipo/shRNA lipoplexes, but no statistical significance was achieved. The spectral unmixing analysis confirmed that the fluorescence measured is the specific signal emitted by Rhodamine B, used to fluorescently label the lipoplexes (Fig. 3A-c). Evidence of successful plasmid DNA (pDNA) delivery after the distribution of lipoplexes in vivo was reported by Mahato et al. [65]. They reported that the most significant quantities of pDNA at 24 h after tail vein injection of lipoplexes were found in the lungs and liver, while in the kidney, spleen, heart, and blood, the amount of pDNA was insignificant. The analysis of the aortas alone revealed a higher radiant efficiency measured in the specimens isolated from mice injected with Psel-lipo/shCTR as compared with mice that received Scr-lipo/shCTR lipoplexes (Figs. 3B-a and 3B-b). The accumulation of Psel-lipo/shRNA at the sites of atherosclerotic plaques was revealed when overlaying the fluorescent images with photographic images taken with the IVIS system (Fig. 3B-c). The administration of Psel-lipo/shCTR produced a strong fluorescence that was visualized in the areas with atherosclerotic lesions, having a white opacity appearance due to the lipid-rich content (observed on photographic images). It can be undoubtedly seen that Scr-lipo/shCTR does not associate with these atherosclerotic areas. The spectral unmixing analysis points out the specific localization of Psel-lipo/shCTR in the aortas of ApoE-deficient mice (Fig. 3B-c). By contrast, in the case of Scr-lipo/shCTR administration, no fluorescence specific for the lipoplexes label (Rhodamine B) was detected. These data demonstrate that i.v. administration of lipoplexes directed to P-selectin by coupling the recognizing peptide, results in their localization at the atherosclerotic plaque and vascular areas with inflamed endothelium, exhibiting increased expression of P-selectin. Considering the protocol, which required thorough washing of the vasculature with a peristaltic pump injecting cold PBS (at a rate of 2.5 ml/min) in the left ventricle, we can assume that the Scr-lipo/shRNA lipoplexes were washed away, while the interaction between the Psel-lipo/shRNA lipoplexes with P-selectin expressed on the surface of endothelial cells resisted the artificial shear flow and resulted in the tethering of lipoplexes at the vascular lesions.

However, since the presence of soluble P-selectin (sP-selectin)

circulating in the plasma was reported [66], there is a possibility that a certain amount of peptide exposed by lipoplexes binds to sP-selectin and this might interfere with the binding of P-selectin targeted lipoplexes to the endothelium. Elevated levels of sP-selectin in ApoE-deficient mice (256 ± 37 ng/ml) were detected, but these were not significantly different from the wild-type mice (127 ± 10 ng/ml) [66]. Nevertheless, our data showed that targeted lipoplexes could find and bind to their target on the activated endothelium surface. We administered approximately 0.2 μmol lipid/ 2 μg P-selectin binding peptide/ml, which is 10-fold higher than the reported sP-selectin, and it appears that this level is enough for the specific binding of Psel-lipo/shRNA lipoplexes to the atherosclerotic sites.

3.3.2. *In vivo transfection efficiency of P-selectin targeted lipoplexes*

The ability of P-selectin targeted lipoplexes to efficiently deliver the plasmid to the cells of the arterial wall was investigated using the pEYFP plasmid containing a reporter gene encoding the enhanced yellow fluorescent protein (EYFP). The transfection efficacy was further investigated by the specific fluorescent signal identified in the aorta and organs of ApoE-deficient mice, at 72 h after one single i.v. injection with targeted (Psel-lipo/pEYFP) or non-targeted (Scr-lipo/pEYFP) lipoplexes made with the pEYFP plasmid (1.5 mg/kg body weight).

We have found that both the targeted and the non-targeted lipoplexes induced the expression of the fluorescent protein reporter gene in the lungs of ApoE-deficient mice, with no significant differences in EYFP expression between the two experimental groups (Fig. 3C-a, b).

Previous studies reported that i.v. administration of lipoplexes leads to their accumulation at a higher extent within the lung, namely ~80% of the injected dose being localized in this organ. Consequently, high levels of gene expression were reported for lungs in the case of in vivo transfection using lipoplexes [67,68]. This explains our data showing the accumulation of the lipoplexes and the expression of EYFP in the lungs. Alternatively, a possible explanation of the fact that P-selectin targeted lipoplexes did not induce a higher level of fluorescent protein expression could be that the retention of lipoplexes, irrespective of formulation, in the lungs is a consequence of the first-pass phenomenon, as it is the first capillary bed encountered after i.v. retro-orbital injection [69]. Indeed, our biodistribution studies showed that at one hour after injection, the level of accumulation in the lungs was similar for both lipoplexes formulations (Fig. 3A-b). Moreover, it was reported that the retention of lipoplexes in the lungs for approximately one hour is central for the high levels of expression determined [70].

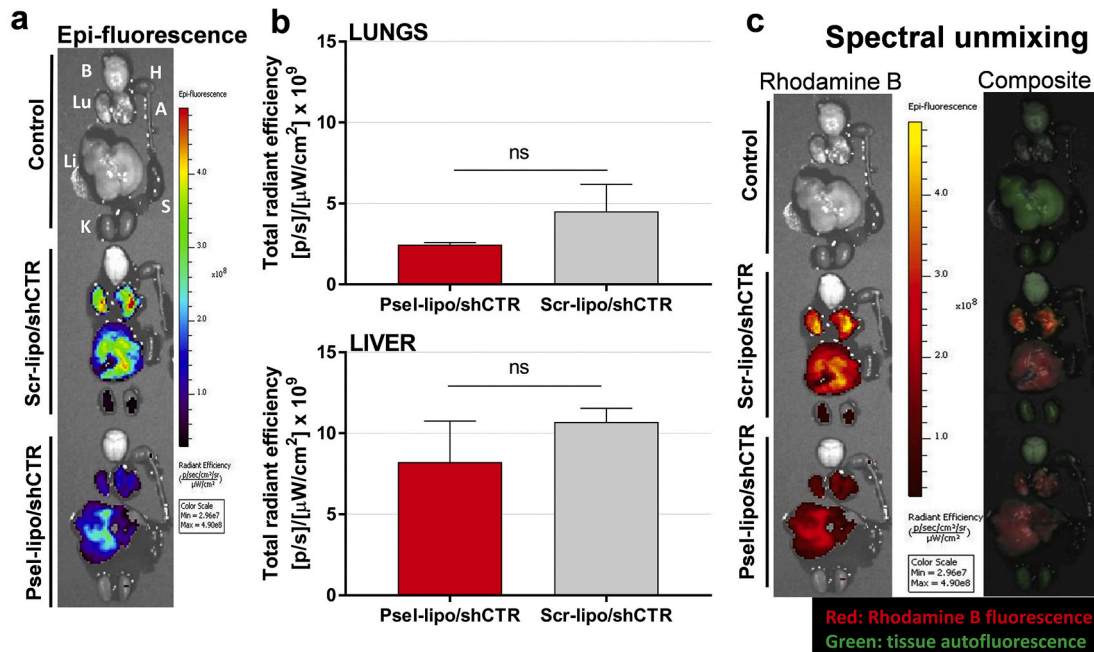
A statistically significant increase in EYFP expression was measured in the aorta of mice receiving Psel-lipo/pEYFP (by 2-fold, $p = 0.006$) as compared to Scr-lipo/pEYFP (Fig. 3C-a, b). Spectral unmixing analysis confirmed the specific expression of the fluorescent protein in the aortas of mice injected with Psel-lipo/pEYFP (Fig. 3C-c).

It has been previously described that vascular EC efficiently internalize efficiently lipoplexes [71–73]. They are able to appropriately traffic and express the delivered gene, after i.v. administration of lipoplexes, with higher efficacy as compared to other cell types such as pulmonary epithelial cells [74].

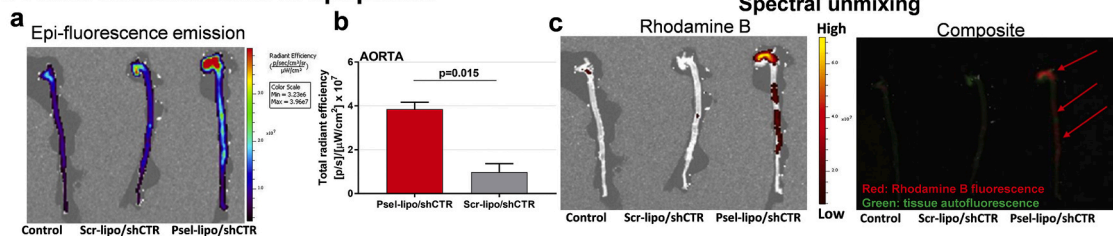
3.3.3. *In vivo downregulation of RAGE by Psel-lipo/shRAGE lipoplexes*

The dose of RAGE-shRNA plasmids chosen for i.v. administration to mice was 1.5 mg/kg since higher doses (2.3 mg/kg) induced the proinflammatory cytokine production [75] and more than 4 mg/kg pDNA provoked morbidity and mortality in mice [76]. Several studies support the 1 mg pDNA/kg dose as effective, without detrimental effects [77,78]. The identical mix of five RAGE-shRNA plasmids, validated in vitro to silence RAGE in mouse EC were employed to obtain P-selectin targeted (Psel-lipo/shRAGE) or non-targeted (Scr-lipo/shRAGE) lipoplexes. A control shRNA plasmid (shCTR) was used to produce P-selectin targeted, non-specific lipoplexes (Psel-lipo/shCTR). The lipoplexes were i.v. administered in ApoE-deficient mice kept on HFD twice a week for four weeks. At the end of the treatment, the aorta,

A: Organ distribution of lipoplexes



B: Aorta accumulation of lipoplexes



C: Fluorescent protein expression

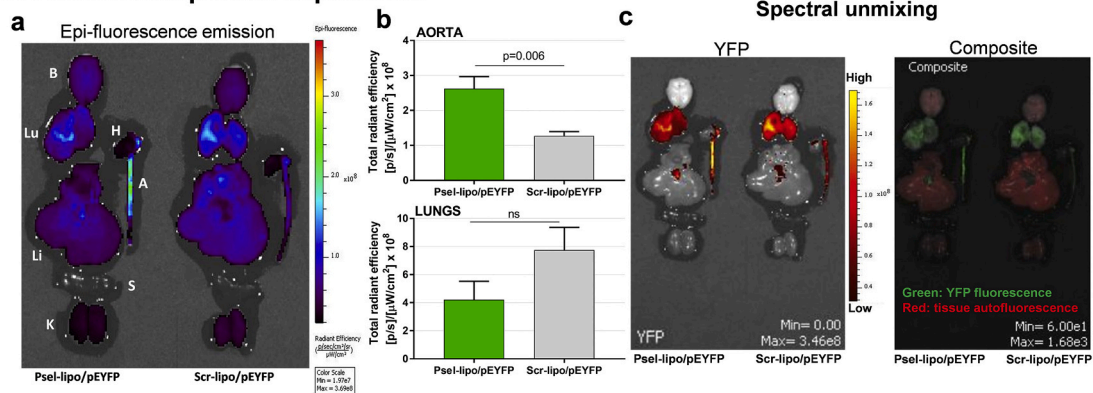


Fig. 3. Localization of Rhodamine B-labeled P-selectin targeted lipoplexes (Psel-lipo/shCTR) and non-targeted lipoplexes (Scr-lipo/shCTR) in different organs (B: brain, Lu: lungs, H: heart, A: aorta, Li: liver, S: spleen and K: kidneys) (A) and in the aortas (B) harvested from ApoE-deficient mice. The analysis was done one hour after retro-orbital administration of lipoplexes in mice ($n = 3/\text{experimental group}$) using the imaging system IVIS Caliper 200, by detection of Rhodamine B fluorescence at $\lambda_{\text{ex}}/\lambda_{\text{em}}$: 535 nm/ 580 nm. (A) Organ distribution of lipoplexes. (A-a) Fluorescence emission of organs; (A-b) Quantification of total radiant efficiency in the lungs and liver; (A-c) Spectral unmixing analysis to delineate the signal specific for Rhodamine B fluorescence and tissue autofluorescence. The composite image displays Rhodamine B fluorescence (red) and tissue autofluorescence (green). (B) Aorta accumulation of lipoplexes. (B-a) Qualitative analysis of the epi-fluorescence emission signal of the aortas investigated at $\lambda_{\text{ex}}/\lambda_{\text{em}}$: 535 nm/ 580 nm; (B-b) Quantification of total radiant efficiency in the aortas; (B-c) Spectral unmixing analysis to eliminate the tissue autofluorescence signal. The accumulation of Psel-lipo/shRNA at the sites with atherosclerotic lesions can be observed in the left image. The right image shows the fluorescence specific for Rhodamine B signal (red, arrows) and tissue autofluorescence (green). (C) Expression of yellow fluorescent protein (YFP) at 48 h after Psel-Lipo/pEYFP and Scr-lipo/pEYFP administration in ApoE-deficient mice ($n = 3/\text{group}$), detected using the IVIS imaging system at $\lambda_{\text{ex}}/\lambda_{\text{em}}$: 500 nm/ 540 nm. As control, a mouse which received a retro-orbital injection of PBS was used. (C-a) Epi-fluorescence emission of organs; (C-b) Quantification of total radiant efficiency in the aorta and lungs; (C-c) Spectral unmixing analysis. The left image shows the specific expression of YFP in the aorta and lungs and the composite image displays YFP fluorescence (green) and tissue autofluorescence (red). (For interpretation of the references to colour in this figure legend, the reader is referred to the web version of this article.)

lungs, liver and kidneys were investigated for RAGE expression by Western blot.

RAGE comprises several distinct protein domains: (1) an extracellular region (amino acids (aa) between 1 and 342) including a signal peptide (aa: 1–22), followed by three immunoglobulin (Ig)-like domains, one Ig-like V-type domain involved in the ligand binding (aa 23–116) and two Ig-like C2-type domains (aa 124–221 and aa 227–317); (2) a single transmembrane domain (aa 343–363) and (3) a short cytoplasmic tail (aa 364–404) [79]. In our study, we used the mouse monoclonal antibody (A-9, Santa Cruz, cat no. sc-365,154), specific for an epitope located between aa 23–43 in the Ig-like V-type domain, at the N-terminus of RAGE.

As shown in Fig. 4A, the aorta displayed a strong signal of the 46-kDa isoform. A significant downregulation of the RAGE protein expression was obtained when the ApoE-deficient mice were treated with Psel-lipo/shRAGE, as compared with the RAGE expression in the aortas isolated from mice from other groups, namely the Scr-lipo/shRAGE, Psel-lipo/shCTR or PBS group. Neither of the other treatments did significantly downregulate the expression of RAGE in the aorta.

These immunoblot results were strengthened by the immunofluorescence analysis performed on cryosections of the aortic root, isolated from mice from different experimental groups. We found a reduction in RAGE staining on the aortic sections obtained from mice that received Psel-lipo/shRAGE. That was in contrast with the more pronounced staining for RAGE in the aorta sections collected from mice in the control group (PBS) or that from mice in the Scr-lipo/shRAGE and Psel-lipo/shCTR (Fig. 4B).

In the lungs, liver and kidneys, Western blot assays revealed several bands identified by the monoclonal antibody used (Fig. 4C), indicating a complex expression pattern of RAGE isoforms. Several alternative splicing variants have been described for the murine RAGE [80,81] that lead to the main isoforms of RAGE protein, namely the full length protein, the N-truncated isoform (that lack the N-terminal V-type immunoglobulin-like domain) and the secretory, C-truncated (that lack C-terminal transmembrane sequence) isoform [82]. Besides, RAGE has two sites of N-glycosylation [83,84] and it is also proteolytically processed [85,86]. Thus, the observed bands in the homogenates of organs may be explained by these features.

We detected three specific bands for RAGE at molecular masses between 40 and 60 kDa, corresponding to the previously reported RAGE isoforms [84,87]. A comprehensive study on the expression of different isoforms of RAGE in various mouse tissues and cells was done by Gefer J et al. [84]. This study reported protein bands with apparent molecular masses of 57.4, 52.6, and 45.1 kDa proteins in lung lysates of C57BL/6 mice identified as xRAGE, membrane (m)RAGE, and soluble (s)RAGE, respectively. In addition, the study confirmed that both xRAGE and mRAGE were membrane-bound RAGE isoforms. In our study, we also identified the same bands at apparent molecular masses of 55, 50 and 46 kDa. Moreover, we detected two additional bands below 35 kDa in the lungs, liver and kidneys of 28 week-old ApoE-deficient mice kept on HFD for the last four weeks. These bands could correspond to isoforms without the Ig-like C2 domains, transmembrane and cytosolic domains, still containing the ligand binding domain recognized by the antibody used. Nevertheless, it is expected that these isoforms do not have an impact on RAGE signaling since they lack the cytoplasmic domain of the receptor.

The densitometric measurements of RAGE in each organ was done by including in the analysis all the bands detected or the three bands corresponding to the isoforms expressed in the range of 40–60 kDa. The graphs are shown in the Fig. 4C below the Western blots.

In the lungs, the densitometric analysis of all bands identified showed that the administration of Psel-lipo/shCTR caused a statistically significant increase (~85%, $p < 0.05$) in RAGE isoforms as compared to the levels measured in control mice that received PBS (Fig. 4C). Treatment with Scr-lipo/shRAGE determined a statistically significant reduction of RAGE isoforms as compared with that observed in mice

treated with Psel-lipo/shCTR lipoplexes (Fig. 4C). The analysis of the three RAGE protein isoforms with apparent molecular weights of 46 kDa, 50 kDa, and 55 kDa revealed that their expression was significantly decreased by non-targeted Scr-lipo/shRAGE lipoplexes treatment when compared with all the other experimental groups (Supplementary Fig. S2). This observation could be explained by the results showing a higher localization (Fig. 3A) and transfection efficacy (Fig. 3C) in the lungs of the mice injected with non-targeted Scr-lipo/shRAGE lipoplexes in comparison with targeted Psel-lipo/shRAGE lipoplexes, although no statistically significant difference was achieved in those experiments. Apparently, the passive retention of non-targeted lipoplexes in the lungs of mice from the Scr-lipo/shRAGE group produced a downregulation of RAGE isoforms as compared to the Psel-lipo/shCTR and PBS groups.

An increase in RAGE isoforms was also detected in the liver of mice receiving Psel-lipo/shCTR lipoplexes. The RAGE protein isoforms level was significantly higher than the level of RAGE isoforms in mice injected with Psel-lipo/shRAGE (~ 50%, $p < 0.05$). No difference between control mice that received PBS and other experimental groups was detected. It is difficult to explain the increases of RAGE isoform in the liver and lungs when the plasmid shRNA control was injected. One explanation could be that cationic lipids can induce a non-specific increase in gene expression by activating some gene promoters [88]. When using lipoplexes carrying the shRAGE plasmid, this effect is not obvious since the downregulation of RAGE is assured by the shRNA-RAGE. Nevertheless, such an increase was not found for the aortas (Fig. 4A).

In the kidneys, the administration of any type of lipoplexes does not change the RAGE protein isoforms expression (Fig. 4C). Moreover, in the kidneys, the biodistribution and in vivo transfection studies showed no differences between the experimental groups receiving different lipoplexes formulations.

3.3.4. *NF- κ B and TNF- α levels are decreased in the aorta of ApoE-deficient mice treated with Psel/shRAGE lipoplexes*

RAGE is expressed on various cell types implicated in the atherosclerotic plaque formation, i.e. vascular or immune cells [3], and is crucially involved in the inflammatory process associated with the progression of atherosclerosis [4,5]. Binding of various ligands to RAGE activates multiple signaling transduction pathways that finally generate an increased expression of transcription factors, such as NF- κ B, AP-1 and STAT3, which play a central role in the production of proinflammatory cytokines and chemokines [4].

In an attempt to decrease the vascular inflammation in atherosclerosis, we envisaged the downregulation of RAGE expression by specially designed targeted nanoparticles. Immunoblotting experiments were carried out to evaluate the expression of the transcription factor NF- κ B and the cytokine TNF- α in the aorta, after the administration of Psel-lipo/shRAGE. We found that the NF- κ B expression at protein level was significantly reduced upon i.v. injection of Psel-lipo/shRAGE lipoplexes (~ 60–70%, $p < 0.05$) as compared with the levels obtained in the aortas from ApoE-deficient mice having received Scr-lipo/shRAGE, Psel-lipo/shCTR or PBS (Fig. 5A). The immunofluorescence analysis of the aortic root supported the immunoblotting results. We detected fainter staining for NF- κ B on the cryosections of aorta isolated from ApoE-deficient mice that had received Psel-lipo/shRAGE as compared to similar sections from mice from the control group (PBS) or from the Scr-lipo/shRAGE and Psel-lipo/shCTR groups (Fig. 5B).

The level of TNF- α , whose expression is induced by NF- κ B, was also significantly decreased by ~60% in the homogenates of aortas from mice injected with Psel-lipo/shRAGE in comparison with those from control mice injected with the Scr-lipo/shRAGE lipoplexes or with PBS (Fig. 5A). These data demonstrated that the underlying mechanism of the anti-inflammatory potential of Psel-lipo/shRAGE lipoplexes is the reduction of NF- κ B in the aorta of ApoE-deficient mice.

Our data extend previous studies that reported that i.v. injection, for six weeks, of RAGE-specific siRNA expression vectors in a liver fibrosis rat model effectively inhibits the mRNA NF- κ B expression and decreases

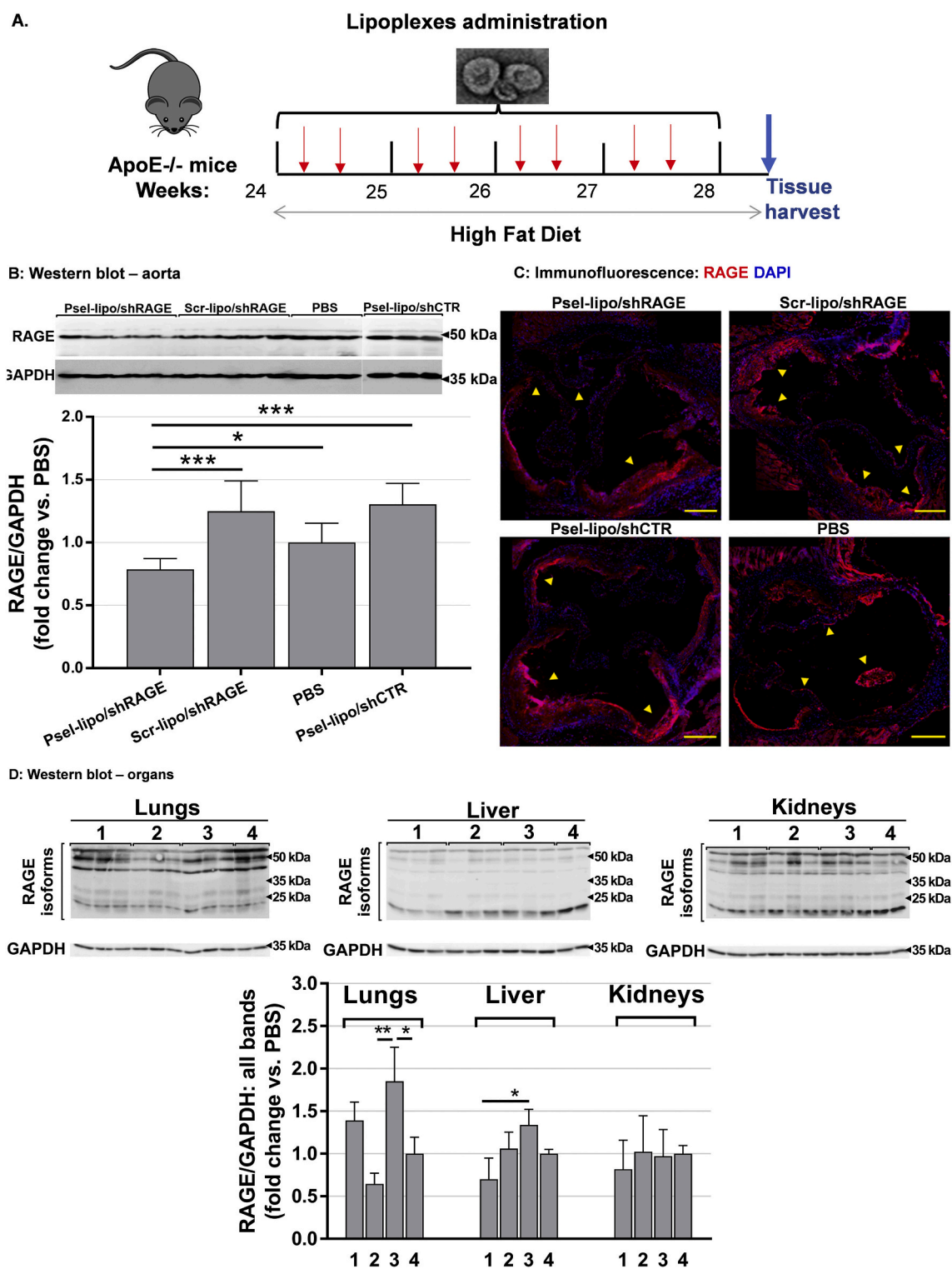


Fig. 4. (A) The schematic representation of in vivo experiments. ApoE-deficient mice were injected twice a week for four weeks with Psel-lipo/shRAGE, Scr-lipo/shRAGE and Psel-lipo/shCTR lipoplexes and simultaneously fed with the HFD ($n = 9$ mice/experimental group). At the end of the experiment, tissues were harvested for investigation. (B) Expression of RAGE in homogenates of aortas from mice treated with lipoplexes (Psel-lipo/shRAGE, Scr-lipo/shRAGE or Psel-lipo/shCTR) normalized to levels measured in control mice (PBS). Data are mean \pm SD; statistical significance: * $p < 0.05$, *** $p < 0.001$. (C) Representative fluorescence micrographs of aortic root cryosections labeled for RAGE (red) and counterstained with DAPI (blue) to identify the nuclei; arrows indicate RAGE-positive areas; scalebar: 100 μ m. (D) Expression of RAGE isoforms in homogenates of lungs, liver and kidneys isolated from mice treated with lipoplexes Psel-lipo/shRAGE (lanes 1), Scr-lipo/shRAGE (lanes 2) or Psel-lipo/shCTR (lanes 3) and PBS (lanes 4). The graph shows data as means \pm SD; statistical significance: * $p < 0.05$, ** $p < 0.01$. (For interpretation of the references to colour in this figure legend, the reader is referred to the web version of this article.)

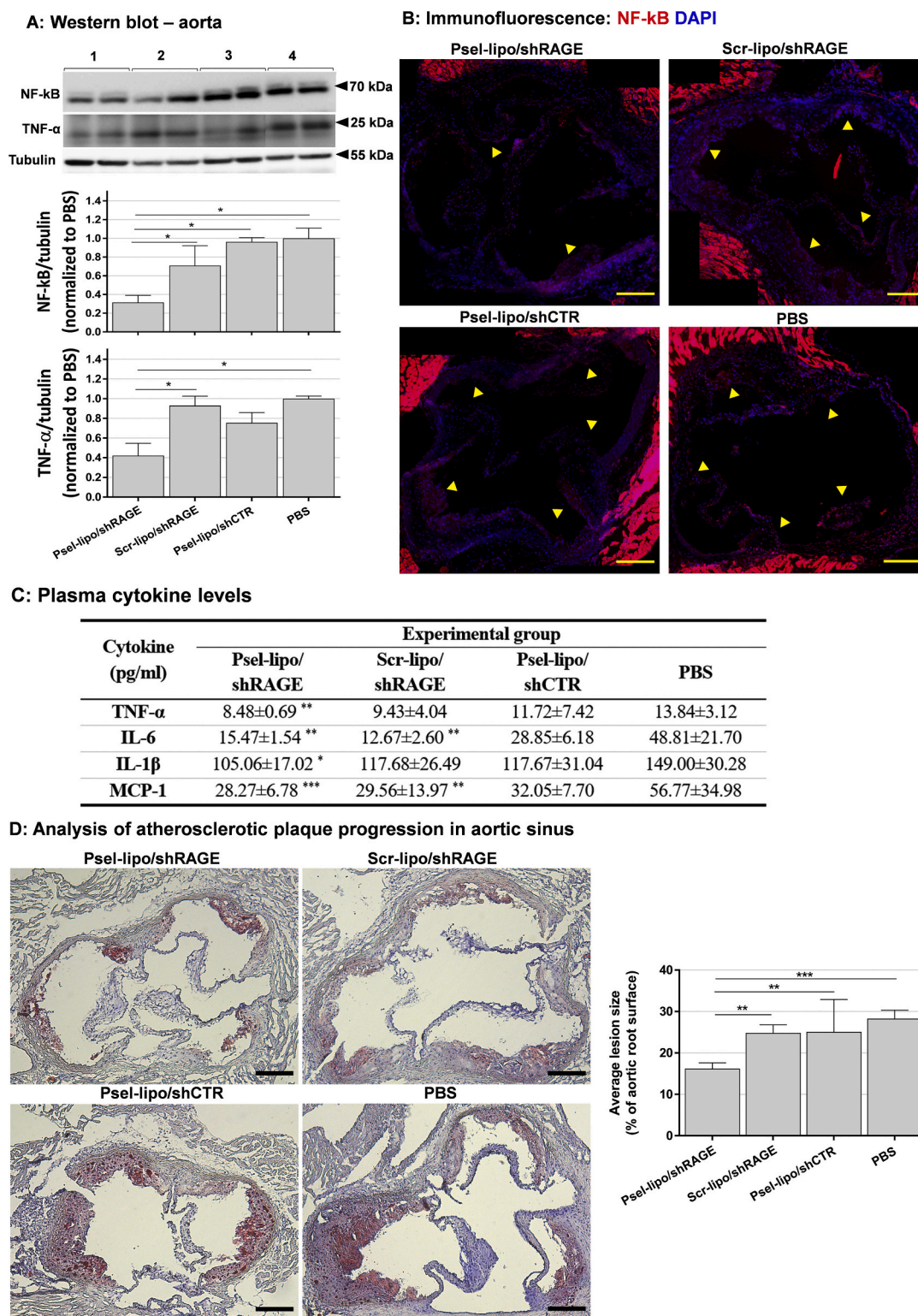


Fig. 5. (A) Western blot assay to evaluate the expression of NF-κB p65 and TNF-α in aorta homogenates from mice treated with Psel-lipo/shRAGE (lanes 1), Scr-lipo/shRAGE (lanes 2) and Psel-lipo/shCTR (lanes 3) or PBS (lanes 4). The graphs present data as means ± SD normalized to tubulin, considering the expression of the proteins in the aorta homogenates of control mice (PBS) as 1 ($n = 6$ mice/experimental group). Statistical significance: * $p < 0.05$. (B) Representative fluorescence micrographs of aortic root cryosections labeled for NF-κB (red) and counterstained with DAPI (blue) to identify the nuclei. The arrows indicate NF-κB-positive areas. Scale bar: 100 μm. At least 3 mice/group were investigated. (C) Cytokine concentrations (pg/ml) in the plasma of the animals injected with lipoplexes or PBS as assessed at the end of the four-week treatment. Values are mean ± SD. Statistical significance: * $p < 0.05$, ** $p < 0.01$, *** $p < 0.001$ versus PBS. (D) Representative images of sections through the aortic sinus collected from mice of different experimental groups stained for lipids with Oil Red O. The graph shows the morphometrical analysis of lesion area calculated as percentage of total aortic root surface area. Data represent the mean values ± SD from Psel-lipo/shRAGE, Scr-lipo/shRAGE, Psel-lipo/shCTR and PBS groups (10 sections/mouse, $n = 6$). Scale bar: 200 μm. ** $p < 0.01$, *** $p < 0.001$. (For interpretation of the references to colour in this figure legend, the reader is referred to the web version of this article.)

serum levels of inflammatory cytokines, including TNF- α and interleukin-6 (IL-6) [89].

3.3.5. Psel-lipo/shRAGE administration reduces plasma levels of inflammatory cytokines in ApoE-deficient mice

Treatment of ApoE-deficient mice kept on HFD with Psel-lipo/shRAGE determined a significant reduction of the plasmatic concentrations of the inflammatory cytokines TNF- α , IL-6, IL-1 β and MCP-1 chemokine, which decreased by ~40% ($p < 0.01$), ~70% ($p < 0.01$), ~30% ($p < 0.05$) and ~50% ($p < 0.001$), respectively, as compared to plasma levels of control mice having received PBS (Fig. 5C). Also, the administration of Scr-lipo/shRAGE lipoplexes induced a reduction of IL-6 (~70%, $p < 0.01$) and MCP-1 (~50%, $p < 0.01$) versus the levels detected in control (PBS-injected) mice. No difference was obtained when the levels of these cytokines detected in the group having received Psel-lipo/shCTR lipoplexes were compared with the values measured in the PBS group (Fig. 5C). We can safely assume that the decreased concentration of plasma cytokines in mice injected with Psel-lipo/shRAGE may be due to the reported down-regulation of RAGE protein expression and decreased NF- κ B levels, in the aorta, with the subsequent reduction of inflammatory cytokine production in the arterial wall. Moreover, the RAGE down-regulation in the lungs and liver can concur to the plasma cytokine levels reduction. The reduction in IL-6 and MCP-1 observed in mice treated with Scr-lipo/shRAGE may be explained by the reduction of RAGE protein levels in lungs that could contribute to the diminished production of these cytokines.

3.3.6. Psel-lipo/shRAGE lipoplexes reduce the atherosclerotic plaque burden

The accumulation of lipids in the aortic root was evaluated comparatively in mice of each experimental groups treated with different types of lipoplexes (Psel-lipo/shRAGE, Scr-lipo/shRAGE, or Psel-lipo/shCTR), and PBS upon staining of the valve cryosections with ORO (Fig. 5D). The morphometric analysis of the cross-sectional area of the aortic sinus covered by lesions indicated a decrease in the atherosclerotic plaque growth in the ApoE-deficient mice treated with Psel-lipo/shRAGE lipoplexes. The lesion area normalized to the aortic root surface was significantly reduced by ~40% ($p < 0.001$) in the Psel-lipo/shRAGE group versus the PBS control group, and by ~30% versus the Scr-lipo/shRAGE and Psel-lipo/shCTR groups ($p < 0.01$) (Fig. 5D). The percentage of inhibition of atherosclerotic plaque development upon the administration of Psel-lipo/shRAGE compared with plaque development in control animals was relatively high (~40%), given that the treatment was performed for only one month in conditions of HFD. The data suggest that a lessening of atherosclerosis by reducing the expression of RAGE in the aorta is feasible. Our results extend previous studies showing that the administration of the soluble isoform of RAGE (sRAGE) in ApoE-deficient mice prevents the development and progression of atherosclerosis in this animal model [90]. In another study, sRAGE administration in diabetic ApoE-deficient mice halted the lesion progression by blocking the influx of macrophages and inhibiting the proliferation of smooth muscle cells in the atherosclerotic lesions [11].

3.3.7. The administration of Psel-lipo/shRAGE lipoplexes displays no toxicity profile

To monitor animal welfare throughout the in vivo experiment, we examined the weight fluctuations, the body postures and behavior, as described in the animal-based assessment welfare methods [91,92]. The weight of the mice varied insignificantly (less than 5% of the initial weight) during the four weeks of the experiments (Fig. 6A). Also, their behavior remained unaltered and the body postures was not indicative of physical pain.

The toxicity of lipoplexes was assessed by biochemistry assays [93]. The plasmatic concentrations of cholesterol and triglycerides were expected to be high and maintain constant in all the experimental groups, as a consequence of the continuous administration of the HFD

throughout the four-week treatment period. No significant differences in these two biochemical parameters were observed between the experimental groups treated with different types of lipoplexes (Fig. 6B). Also, the hepatic function assessed by measuring ALT and AST enzymes, and the renal function investigated by quantification of blood urea nitrogen (BUN) and creatinine, showed no significant alterations among the experimental groups (Fig. 6B). No evidence of hepatic and renal damage was observed after one-month of treatment with lipoplexes, as indicated by the levels of the investigated parameters that are not significantly different from those in control, ApoE-deficient mice having received PBS.

Histology analysis of organs performed on hematoxylin-eosin staining - sections showed no significant abnormalities in the lungs, liver and kidneys morphology in the mice having received Psel-lipo/shRAGE (Fig. 6C). Though, of all experimental groups, in the mice having received the Psel-lipo/shCTR lipoplexes, the thickening of alveolar septal (Fig. 6D) without inflammatory cell infiltrates (Fig. 6E) was observed. This was possible due to septal edema induced by unidentified off-target effects of the control shRNA plasmid that increased the expression of RAGE isoforms as compared with other experimental groups (Fig. 4C).

The hemocompatibility tests showed that the percentages of lysed erythrocytes after incubation with lipoplexes is ~2%, less than the 5% threshold (Fig. 6F), that is considered the safe hemolytic ratio for biomaterials, according to International Organization for Standardization (ISO) 10,993-4:2017. In addition, the examination of the erythrocytes after incubation with lipoplexes does not reveal any aggregation, the appearance being similar to the negative control (incubation in PBS) (Fig. 6G).

4. Conclusions

We developed lipoplexes targeted to P-selectin to efficiently deliver RAGE-shRNA to the atherosclerotic plaque in order to decrease the inflammatory process and the ensuing lesion development. In vitro, Psel-lipo/shRAGE lipoplexes were efficiently taken up by activated EC, decreased the expression of RAGE protein and had a functional role in reducing the monocyte adhesion to activated EC. In vivo, in a mouse model of atherosclerosis (ApoE-deficient mice), the targeted lipoplexes accumulated specifically and efficiently transfected the aorta. The repeated administration of Psel-lipo/shRAGE lipoplexes (i) reduced the expression of RAGE protein in the aorta by decreasing the expression of NF- κ B and TNF- α ; (ii) diminished the plasma levels of TNF- α , IL-6, IL-1 β , and MCP-1; (iii) inhibited the atherosclerotic plaque development and (iv) had no significant adverse effects. Together, these data suggest that the newly developed Psel-lipo/shRAGE lipoplexes represent a promising novel targeted therapy to block the progression of atherosclerosis.

Data availability statement

The data that support the findings of this study are available from the corresponding author upon request.

Ethical approval

All animal experiments were approved by the Ethics Committee of the Institute of Cellular Biology and Pathology “Nicolae Simionescu” and by the National Sanitary Veterinary and Food Safety Authority authorization no. 295/23.08.2016 and were performed in accordance with the Romanian Law no. 43/2014 (Official Monitor, Part I nr. 326: p 2–4.), which transposes the EU directive 2010/63/EU on the protection of animals used for scientific purposes.

Declaration of Competing Interest

The authors declare that they do not have a competing interest

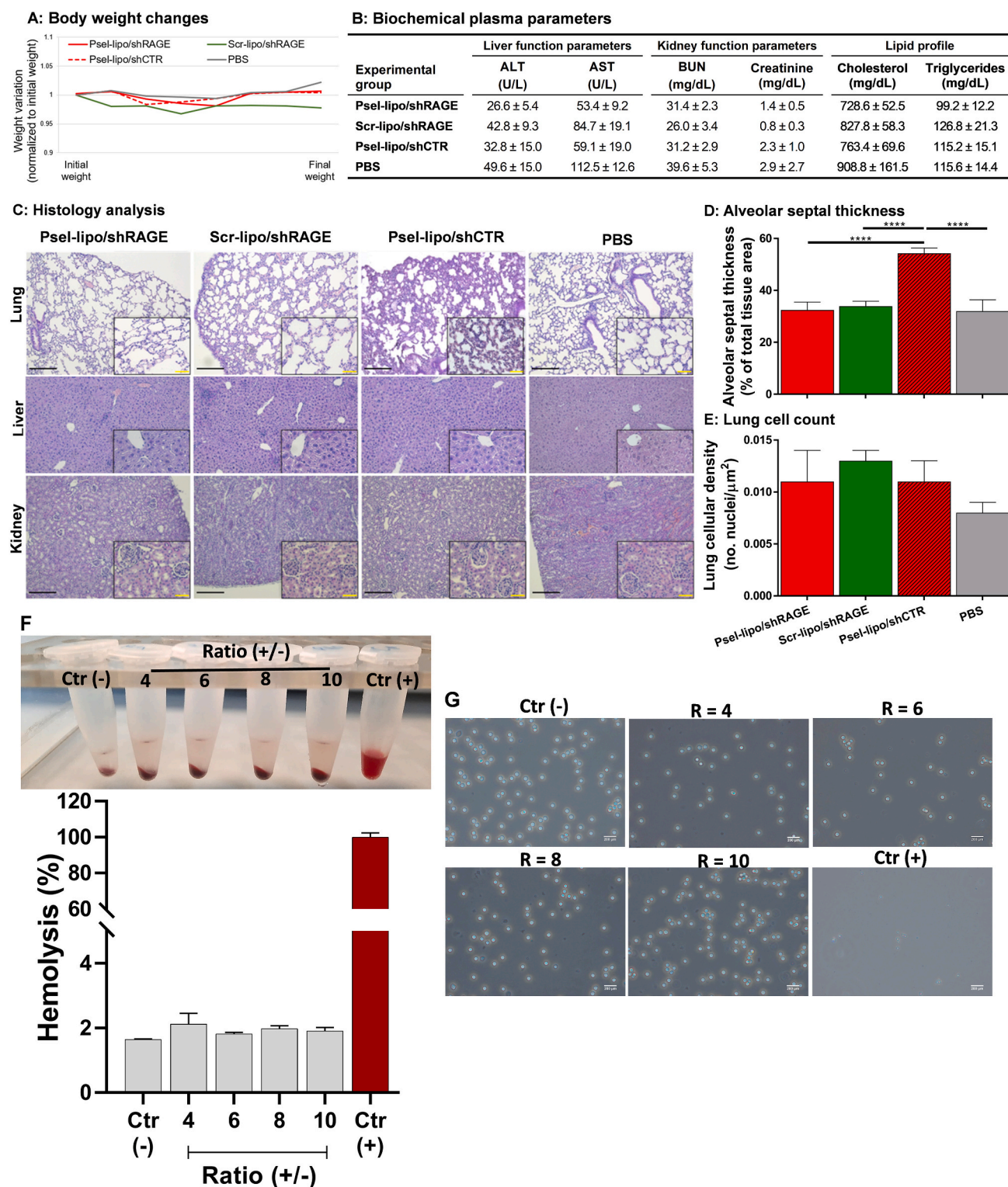


Fig. 6. Safety assessment of the effects of lipoplexes administered in vivo. **(A)** Variation in body weight of mice from different groups during experiment. **(B)** Biochemical parameters for liver function (ALT, AST), kidney function (BUN and creatinine) and the lipid profile (cholesterol, triglycerides) measured in the plasma of control mice (PBS) or mice treated with lipoplexes (Psel-lipo/shRAGE, Scr-lipo/shRAGE, Psel-lipo/shCTR) at the end of the four-week treatment. Data are mean ± SD ($n = 9$ mice for each group). **(C)** Histology (H&E staining) of organs collected from control mice (PBS) or mice treated with various formulations of lipoplexes (Psel-lipo/shRAGE, Scr-lipo/shRAGE, Psel-lipo/shCTR) for one-month (main panel scale bar (black): 200 μm , inset scale bar (yellow): 50 μm). **(D)** Alveolar wall thickness and **(E)** Lung cellularity measurement on images taken using x20 objective ($n = 3$ mice were analyzed for each group, and 10 random fields per mouse were used for analysis using ImageJ 1.53c Macros described in Supplementary Material). **(F)** Quantification of hemolysis in erythrocytes incubated with Psel-lipo/shCTR plasmid at different charge ratios (R). The corresponding photographs after erythrocytes sedimentation upon exposure to various experimental conditions are shown above. **(G)** Evaluation of erythrocyte aggregation after incubation with lipoplexes, PBS [Ctr (-)] and 0.5% Triton X-100 [Ctr (+)]. Scale bar: 200 μm . (For interpretation of the references to colour in this figure legend, the reader is referred to the web version of this article.)

concerning the publication of this paper.

Acknowledgments

The authors are indebted to Dr. Mihaela Gherghiceanu, “Victor Babes” National Institute of Pathology for TEM investigations. We gratefully thank the staff of the SPF Animal Facility at the Institute of Cellular Biology and Pathology for providing technical support.

The work was supported in part by grants from the Romanian Ministry of Education and Research, CNCS – UEFISCDI (project numbers PN-II-RU-TE-2014-4-1837, PN-III-P4-ID-PCCF-2016-0050 and PN-III-P4-ID-PCE-2020-2465) and the EU Competitiveness Operational Programme 2014-2020, Priority Axis1/Action 1.1.4 contract no. 115/13.09.2016/MySMIS:104362.

Appendix A. Supplementary data

Supplementary data to this article can be found online at <https://doi.org/10.1016/j.jconrel.2021.09.012>.

References

- Calin, I. Manduteanu, Emerging nanocarriers-based approaches to diagnose and reduce vascular inflammation in atherosclerosis, *Curr. Med. Chem.* 24 (2017) 550–567, <https://doi.org/10.2174/0929867324666161123091627>.
- S. Del Turco, G. Basta, An update on advanced glycation endproducts and atherosclerosis, *BioFactors*. 38 (2012) 266–274, <https://doi.org/10.1002/biof.1018>.
- A.M. Schmidt, 2016 ATVB plenary lecture, *Arterioscler. Thromb. Vasc. Biol.* 37 (2017) 613–621, <https://doi.org/10.1161/ATVB.AHA.117.307263>.
- E. Harja, D. Bu, B.I. Hudson, J.S. Chang, X. Shen, K. Hallam, A.Z. Kalea, Y. Lu, R. H. Rosario, S. Oruganti, Z. Nikolla, D. Belov, E. Lalla, R. Ramasamy, S.F. Yan, A. M. Schmidt, Vascular and inflammatory stresses mediate atherosclerosis via RAGE and its ligands in apoE^{-/-} mice, *J. Clin. Invest.* 118 (2008) 183–194, <https://doi.org/10.1172/JCI32703>.
- S.F. Yan, R. Ramasamy, A.M. Schmidt, The RAGE axis, *Circ. Res.* 106 (2010) 842–853, <https://doi.org/10.1161/CIRCRESAHA.109.212217>.
- A.M. Schmidt, O. Hori, J.X. Chen, J.F. Li, J. Crandall, J. Zhang, R. Cao, S.D. Yan, J. Brett, D. Stern, Advanced glycation endproducts interacting with their endothelial receptor induce expression of vascular cell adhesion molecule-1 (VCAM-1) in cultured human endothelial cells and in mice. A potential mechanism for the accelerated vasculopathy of diabetes, *J. Clin. Invest.* 96 (1995) 1395–1403, <https://doi.org/10.1172/JCI18175>.
- L. Lin, RAGE signaling in inflammation and arterial aging, *Front. Biosci.* 1403 (2009), <https://doi.org/10.2741/3315>.
- T. Chavakis, A. Bierhaus, N. Al-Fakhri, D. Schneider, S. Witte, T. Linn, M. Nagashima, J. Morser, B. Arnold, K.T. Preissner, P.P. Nawroth, The pattern recognition receptor (RAGE) is a Counterreceptor for leukocyte Integrins, *J. Exp. Med.* 198 (2003) 1507–1515, <https://doi.org/10.1084/jem.20030800>.
- V.V. Orlova, E.Y. Choi, C. Xie, E. Chavakis, A. Bierhaus, E. Ihanus, C.M. Ballantyne, C.G. Gahmberg, M.E. Bianchi, P.P. Nawroth, T. Chavakis, A novel pathway of HMGB1-mediated inflammatory cell recruitment that requires mac-1-integrin, *EMBO J.* 26 (2007) 1129–1139, <https://doi.org/10.1038/sj.emboj.7601552>.
- F. Cipollone, A. Iezzi, M. Fazio, M. Zucchelli, B. Pini, C. Cucurullo, D. De Cesare, G. De Blasis, R. Muraro, R. Bei, F. Chiarelli, A.M. Schmidt, F. Cucurullo, A. Mezzetti, The receptor RAGE as a progression factor amplifying Arachidonate-dependent inflammatory and Proteolytic response in human atherosclerotic plaques, *Circulation*. 108 (2003) 1070–1077, <https://doi.org/10.1161/01.CIR.0000086014.80477.0D>.
- L.G. Bucciarelli, T. Wendt, W. Qu, Y. Lu, E. Lalla, L.L. Rong, M.T. Goova, B. Moser, T. Kislinger, D.C. Lee, Y. Kashyap, D.M. Stern, A.M. Schmidt, RAGE blockade stabilizes established atherosclerosis in diabetic Apolipoprotein E-null mice, *Circulation*. 106 (2002) 2827–2835, <https://doi.org/10.1161/01.CIR.0000039325.03698.36>.
- A. Soro-Paavonen, A.M.D. Watson, J. Li, K. Paavonen, A. Koitka, A.C. Calkin, D. Barit, M.T. Coughlan, B.G. Drew, G.I. Lancaster, M. Thomas, J.M. Forbes, P. P. Nawroth, A. Bierhaus, M.E. Cooper, K.A. Jandeleit-Dahm, Receptor for advanced Glycation end products (RAGE) deficiency attenuates the development of atherosclerosis in diabetes, *Diabetes*. 57 (2008) 2461–2469, <https://doi.org/10.2337/db07-1808>.
- S. Morris-Rosenfeld, E. Blessing, M.R. Preusch, C. Albrecht, A. Bierhaus, M. Andrassy, P.P. Nawroth, M.E. Rosenfeld, H.A. Katus, F. Beja, Deletion of bone marrow-derived receptor for advanced glycation end products inhibits atherosclerotic plaque progression, *Eur. J. Clin. Invest.* 41 (2011) 1164–1171, <https://doi.org/10.1111/j.1365-2362.2011.02514.x>.
- Q. Fan, J. Liao, M. Kobayashi, M. Yamashita, L. Gu, T. Gohda, Y. Suzuki, L. N. Wang, S. Horikoshi, Y. Tomino, Candesartan reduced advanced glycation end-products accumulation and diminished nitro-oxidative stress in type 2 diabetic KK/ta mice, *Nephrol. Dial. Transplant.* 19 (2004) 3012–3020, <https://doi.org/10.1093/ndt/gfh499>.
- K. Nakamura, S. Yamagishi, Y. Nakamura, K. Takenaka, T. Matsui, Y. Jinnouchi, T. Imaizumi, Telmisartan inhibits expression of a receptor for advanced glycation end products (RAGE) in angiotensin-II-exposed endothelial cells and decreases serum levels of soluble RAGE in patients with essential hypertension, *Microvasc. Res.* 70 (2005) 137–141, <https://doi.org/10.1016/j.mvr.2005.10.002>.
- C. Cucurullo, A. Iezzi, M.L. Fazio, D. De Cesare, A. Di Francesco, R. Muraro, R. Bei, S. Uchino, F. Spigonardo, F. Chiarelli, A.M. Schmidt, F. Cucurullo, A. Mezzetti, F. Cipollone, Suppression of RAGE as a basis of simvastatin-dependent plaque stabilization in type 2 diabetes, *Arterioscler. Thromb. Vasc. Biol.* 26 (2006) 2716–2723, <https://doi.org/10.1161/01.ATV.0000249630.02085.12>.
- K. Wang, Z. Zhou, M. Zhang, L. Fan, F. Forudi, X. Zhou, W. Qu, A.M. Lincoff, A. M. Schmidt, E.J. Topol, M.S. Penn, Peroxisome proliferator-activated receptor γ Down-regulates receptor for advanced Glycation end products and inhibits smooth muscle cell proliferation in a diabetic and nondiabetic rat carotid artery injury model, *J. Pharmacol. Exp. Ther.* 317 (2006) 37–43, <https://doi.org/10.1124/jpet.105.095125>.
- L. Xu, P. Zang, B. Feng, Q. Qian, Atorvastatin inhibits the expression of RAGE induced by advanced glycation end products on aortas in healthy Sprague–Dawley rats, *Diabetol. Metab. Syndr.* 6 (2014) 102, <https://doi.org/10.1186/1758-5996-6-102>.
- W. Wei, M. Chen, Y. Zhu, J. Wang, P. Zhu, Y. Li, J. Li, Down-regulation of vascular HMGB1 and RAGE expression by n-3 polyunsaturated fatty acids is accompanied by amelioration of chronic vasculopathy of small bowel allografts, *J. Nutr. Biochem.* 23 (2012) 1333–1340, <https://doi.org/10.1016/j.jnutbio.2011.08.002>.
- H. Gao, H. Li, W. Li, X. Shen, B. Di, Pioglitazone attenuates atherosclerosis in diabetic mice by inhibition of receptor for advanced glycation end-product (RAGE) signaling, *Med. Sci. Monit* 23 (2017) 6121–6131, <https://doi.org/10.12659/MSM.907401>.
- P. Li, Z. Tang, L. Wang, B. Feng, Glucagon-like peptide-1 analogue liraglutide ameliorates atherogenesis via inhibiting advanced glycation end product-induced receptor for advanced glycosylation end product expression in apolipoprotein-E deficient mice, *Mol. Med. Rep.* 16 (2017) 3421–3426, <https://doi.org/10.3892/mmr.2017.6978>.
- S. Bongarzone, V. Savickas, F. Luzzi, A.D. Gee, Targeting the receptor for advanced Glycation Endproducts (RAGE): a medicinal chemistry perspective, *J. Med. Chem.* 60 (2017) 7213–7232, <https://doi.org/10.1021/acs.jmedchem.7b00058>.
- V.L.M. Herrera, A.H. Colby, N. Ruiz-Opazo, D.G. Coleman, M.W. Grinstaff, Nucleic acid nanomedicines in phase II/III clinical trials: translation of nucleic acid therapies for reprogramming cells, *Nanomedicine*. 13 (2018) 2083–2098, <https://doi.org/10.2217/nmm-2018-0122>.
- N.I. Khatri, M.N. Rath, D.P. Baradia, S. Trehan, A. Misra, In vivo delivery aspects of miRNA, shRNA and siRNA, *Crit. Rev. Ther. Drug Carr. Syst.* 29 (2012) 487–527, <https://doi.org/10.1615/CritRevTherDrugCarrierSyst.v29.i6.20>.
- M.A. McAnuff, G.R. Rettig, K.G. Rice, Potency of siRNA versus shRNA mediated knockdown in vivo, *J. Pharm. Sci.* 96 (2007) 2922–2930, <https://doi.org/10.1002/jps.20968>.
- B. Moore, L.P. Dasi, Spatiotemporal complexity of the aortic sinus vortex, *Exp. Fluids* 55 (2014) 1770, <https://doi.org/10.1007/s00348-014-1770-0>.
- Y. Zeng, X. Cai, B.R. Cullen, Use of RNA polymerase II to transcribe artificial MicroRNAs, in: *Methods Enzymol*, 2005, pp. 371–380, [https://doi.org/10.1016/S0076-6879\(04\)92022-8](https://doi.org/10.1016/S0076-6879(04)92022-8).
- R.A. Klinghoffer, J. Magnus, J. Schelter, M. Mehaffey, C. Coleman, M.A. Cleary, Reduced seed region-based off-target activity with lentivirus-mediated RNAi, *RNA*. 16 (2010) 879–884, <https://doi.org/10.1261/ma.1977810>.
- D.D. Rao, N. Senzer, M.A. Cleary, J. Nemunaitis, Comparative assessment of siRNA and shRNA off target effects: what is slowing clinical development, *Cancer Gene Ther.* 16 (2009) 807–809, <https://doi.org/10.1038/cgt.2009.53>.
- M.S. Shim, Y.J. Kwon, Efficient and targeted delivery of siRNA in vivo, *FEBS J.* 277 (2010) 4814–4827, <https://doi.org/10.1111/j.1742-4658.2010.07904.x>.
- A. Schlegel, P. Bigey, H. Dhotel, D. Scherman, V. Escriou, Reduced in vitro and in vivo toxicity of siRNA-liposomes with addition of polyglutamate, *J. Control. Release* 165 (2013) 1–8, <https://doi.org/10.1016/j.jconrel.2012.10.018>.
- J.M. Warram, A.G. Sorace, M. Mahoney, S. Samuel, B. Harbin, M. Joshi, A. Martin, L. Whitworth, K. Hoyt, K.R. Zinn, Biodistribution of P-selectin targeted microbubbles, *J. Drug Target.* 22 (2014) 387–394, <https://doi.org/10.3109/1061186X.2013.869822>.
- G. Covarrubias, A. Cha, A. Rahmy, M. Lorkowski, V. Perera, B.O. Erokwu, C. Flask, P.M. Peiris, W.P. Schiemann, E. Karathanasis, Imaging breast cancer using a dual-ligand nanochain particle, *PLoS One* 13 (2018), e0204296, <https://doi.org/10.1371/journal.pone.0204296>.
- V. Simion, C.A. Constantinescu, D. Stan, M. Deleanu, M.M. Tucureanu, E. Butoi, I. Manduteanu, M. Simionescu, M. Calin, P-Selectin targeted dexamethasone-loaded lipid Nanoemulsions: a novel therapy to reduce vascular inflammation, *Mediat. Inflamm.* 2016 (2016) 1–15, <https://doi.org/10.1155/2016/1625149>.
- C.A. Constantinescu, E.V. Fuior, D. Rebleanu, M. Deleanu, V. Simion, G. Voicu, V. Escriou, I. Manduteanu, M. Simionescu, M. Calin, Targeted transfection using PEGylated cationic liposomes directed towards P-Selectin increases siRNA delivery into activated endothelial cells, *Pharmaceutics*. 11 (2019) 47, <https://doi.org/10.3390/pharmaceutics11010047>.
- B. Thompson, N. Mignet, H. Hofland, D. Lamons, J. Seguin, C. Nicolazzi, N. de la Figuera, R.L. Kuen, X.Y. Meng, D. Scherman, M. Bessodes, Neutral Postgrafted colloidal particles for gene delivery, *Bioconjug. Chem.* 16 (2005) 608–614, <https://doi.org/10.1021/bc040244z>.

- [37] T.J.M. Molenaar, J. Twisk, S.A.M. de Haas, N. Peterse, B.J.C.P. Vogelaar, S.H. van Leeuwen, I.N. Michon, T.J.C. van Berkel, J. Kuiper, E.A.L. Biessen, P-selectin as a candidate target in atherosclerosis, *Biochem. Pharmacol.* 66 (2003) 859–866, [https://doi.org/10.1016/S0006-2952\(03\)00387-3](https://doi.org/10.1016/S0006-2952(03)00387-3).
- [38] M. Calin, D. Stan, M. Schlesinger, V. Simion, M. Deleanu, C.A. Constantinescu, A.-M. Gan, M.M. Pirvulescu, E. Butoi, I. Manduteanu, M. Bota, M. Enacescu, L. Borsig, G. Bendas, M. Simionescu, VCAM-1 directed target-sensitive liposomes carrying CCR2 antagonists bind to activated endothelium and reduce adhesion and transmigration of monocytes, *Eur. J. Pharm. Biopharm.* 89 (2015) 18–29, <https://doi.org/10.1016/j.ejpb.2014.11.016>.
- [39] M. Khoury, P. Louis-Pence, V. Escriviou, D. Noel, C. Largeau, C. Cantos, D. Scherman, C. Jorgensen, F. Apparailly, Efficient new cationic liposome formulation for systemic delivery of small interfering RNA silencing tumor necrosis factor α in experimental arthritis, *Arthritis Rheum.* 54 (2006) 1867–1877, <https://doi.org/10.1002/art.21876>.
- [40] G. Voicu, D. Rebleanu, C.A. Constantinescu, E.V. Fuior, L. Ciortan, I. Droc, C. M. Uritu, M. Pinteala, I. Manduteanu, M. Simionescu, M. Calin, Nano-Polyplexes mediated transfection of Runx2-shRNA mitigates the Osteodifferentiation of human Valvular interstitial cells, *Pharmaceutics*. 12 (2020) 507, <https://doi.org/10.3390/pharmaceutics12060507>.
- [41] M.M. Pirvulescu, A.-M. Gan, D. Stan, V. Simion, M. Calin, E. Butoi, C.I. Tirgoviste, I. Manduteanu, Curcumin and a Morus alba Extract reduce pro-inflammatory effects of Resistin in human endothelial cells, *Phyther. Res.* 25 (2011) 1737–1742, <https://doi.org/10.1002/ptr.3463>.
- [42] M.M. Pirvulescu, D. Stan, A.-M. Gan, V. Simion, C. Ionescu-Targoviste, I. Manduteanu, M5402 morus alba extract and curcumin reduce resistin induced-human endothelial cells activation by a mechanism involving P38 MAPK, *Atheroscler. Suppl.* 11 (2010) 191, [https://doi.org/10.1016/S1567-5688\(10\)70903-X](https://doi.org/10.1016/S1567-5688(10)70903-X).
- [43] M.V. Calin, I. Manduteanu, E. Dragomir, E. Dragan, M. Nicolae, A.M. Gan, M. Simionescu, Effect of depletion of monocytes/macrophages on early aortic valve lesion in experimental hyperlipidemia, *Cell Tissue Res.* 336 (2009) 237–248, <https://doi.org/10.1007/s00441-009-0765-2>.
- [44] E. Fuior, M. Deleanu, C. Constantinescu, D. Rebleanu, G. Voicu, M. Simionescu, M. Calin, Functional role of VCAM-1 targeted flavonoid-loaded lipid nanoemulsions in reducing endothelium inflammation, *Pharmaceutics*. 11 (2019) 391, <https://doi.org/10.3390/pharmaceutics11080391>.
- [45] T.G.F. Souza, V.S.T. Ciminelli, N.D.S. Mohallem, A comparison of TEM and DLS methods to characterize size distribution of ceramic nanoparticles, *J. Phys. Conf. Ser.* 733 (2016), 012039, <https://doi.org/10.1088/1742-6596/733/1/012039>.
- [46] A. Congiu, D. Pozzi, C. Esposito, C. Castellano, G. Mossa, Correlation between structure and transfection efficiency: a study of DC-Chol–DOPE/DNA complexes, *Colloids Surfaces B Biointerfaces*. 36 (2004) 43–48, <https://doi.org/10.1016/j.colsurfb.2004.04.006>.
- [47] W. Wan, L. Cao, L. Liu, C. Zhang, B. Kalionis, X. Tai, Y. Li, S. Xia, A β 1–42 oligomer-induced leakage in an in vitro blood-brain barrier model is associated with up-regulation of RAGE and metalloproteinases, and down-regulation of tight junction scaffold proteins, *J. Neurochem.* 134 (2015) 382–393, <https://doi.org/10.1111/jnc.13122>.
- [48] S.A. Ásgeirsdóttir, E.G. Talman, I.A. de Graaf, J.A.A.M. Kamps, S.C. Satchell, P. W. Mathieson, M.H.J. Ruijters, G. Molema, Targeted transfection increases siRNA uptake and gene silencing of primary endothelial cells in vitro — a quantitative study, *J. Control. Release* 141 (2010) 241–251, <https://doi.org/10.1016/j.jconrel.2009.09.008>.
- [49] C.H. Ha, S. Kim, J. Chung, S.H. An, S. Park, D. Choi, K. Kwon, Inhibitory effect of soluble RAGE in disturbed flow-induced atherosclerosis, *Int. J. Mol. Med.* 32 (2013) 373–380, <https://doi.org/10.3892/ijmm.2013.1393>.
- [50] Z.-G. Luan, H. Zhang, P.-T. Yang, X.-C. Ma, C. Zhang, R.-X. Guo, HMGB1 activates nuclear factor- κ B signaling by RAGE and increases the production of TNF- α in human umbilical vein endothelial cells, *Immunobiology*. 215 (2010) 956–962, <https://doi.org/10.1016/j.imbio.2009.11.001>.
- [51] C. Gebhardt, A. Riehl, M. Durchdewald, J. Németh, G. Fürstenberger, K. Müller-Decker, A. Enk, B. Arnold, A. Bierhaus, P.P. Nawroth, J. Hess, P. Angel, RAGE signaling sustains inflammation and promotes tumor development, *J. Exp. Med.* 205 (2008) 275–285, <https://doi.org/10.1084/jem.20070679>.
- [52] Z.M. Dong, A.A. Brown, D.D. Wagner, Prominent role of P-Selectin in the development of advanced atherosclerosis in ApoE-deficient mice, *Circulation*. 101 (2000) 2290–2295, <https://doi.org/10.1161/01.CIR.101.19.2290>.
- [53] R.R. Johnson-Tidey, J.L. McGregor, P.R. Taylor, R.N. Poston, Increase in the adhesion molecule P-selectin in endothelium overlying atherosclerotic plaques: Coexpression with intercellular adhesion molecule-1, *Am. J. Pathol.* 144 (1994) 952–961, <https://www.ncbi.nlm.nih.gov/pmc/articles/PMC1887356/>.
- [54] A. Sakai, N. Kume, E. Nishi, K. Tanoue, M. Miyasaka, T. Kita, P-Selectin and vascular cell adhesion molecule-1 are focally expressed in aortas of Hypercholesterolemic rabbits before intimal accumulation of macrophages and T lymphocytes, *Arterioscler. Thromb. Vasc. Biol.* 17 (1997) 310–316, <https://doi.org/10.1161/01.ATV.17.2.310>.
- [55] K. Woollard, J. Chin-Dusting, Therapeutic targeting of P-Selectin in atherosclerosis, *Inflamm. Allergy-Drug Targets*. 6 (2007) 69–74, <https://doi.org/10.2174/187552807780077345>.
- [56] M.-J. Jacobin-Valat, K. Deramchia, S. Mornet, C.E. Hagemeyer, S. Bonetto, R. Robert, M. Biran, P. Massot, S. Miraux, S. Sanchez, A.-K. Bouzier-Sore, J.-M. Franconi, E. Duguet, G. Clofent-Sanchez, MRI of inducible P-selectin expression in human activated platelets involved in the early stages of atherosclerosis, *NMR Biomed.* 24 (2011) 413–424, <https://doi.org/10.1002/nbm.1606>.
- [57] M.A. McAteer, J.E. Schneider, Z.A. Ali, N. Warrick, C.A. Bursill, C. Von Zur Muhlen, D.R. Greaves, S. Neubauer, K.M. Channon, R.P. Choudhury, Magnetic resonance imaging of endothelial adhesion molecules in mouse atherosclerosis using dual-targeted microparticles of iron oxide, *Arterioscler. Thromb. Vasc. Biol.* 28 (2008) 77–83, <https://doi.org/10.1161/ATVBAHA.107.145466>.
- [58] X. Li, W. Bauer, I. Israel, M.C. Kreissl, J. Weirather, D. Richter, E. Bauer, V. Herold, P. Jakob, A. Buck, S. Frantz, S. Samnick, Targeting P-Selectin by Gallium-68-labeled Fucoidan positron emission tomography for noninvasive characterization of vulnerable plaques, *Arterioscler. Thromb. Vasc. Biol.* 34 (2014) 1661–1667, <https://doi.org/10.1161/ATVBAHA.114.303485>.
- [59] L.A. Perkins, C.J. Anderson, E.M. Novelli, Targeting P-Selectin adhesion molecule in molecular imaging: P-Selectin expression as a valuable imaging biomarker of inflammation in cardiovascular disease, *J. Nucl. Med.* 60 (2019) 1691–1697, <https://doi.org/10.2967/jnumed.118.225169>.
- [60] K.H. Zheng, Y. Kaiser, E. Poel, H. Verberne, J. Aerts, F. Rouzet, E. Stroes, D. Letourneur, C. Chauvierre, 99mTc-Fucoidan as diagnostic agent for P-Selectin imaging: first-in-human evaluation (phase I), *Atherosclerosis*. 287 (2019), e143, <https://doi.org/10.1016/j.atherosclerosis.2019.06.425>.
- [61] K.I. Ataga, A. Kutlar, J. Kanter, D. Liles, R. Friedrisch, T.H. Guthrie, J. Knight-Madden, O.A. Alvarez, V.R. Gordeuk, S. Gualandro, M.P. Colella, W. R. Smith, S.A. Rollins, J.W. Stocker, R.P. Rother, Crizanlizumab for the prevention of pain crises in sickle cell disease, *N. Engl. J. Med.* 376 (2017) 429–439, <https://doi.org/10.1056/NEJMoa1611770>.
- [62] B.E. Stähli, C. Gebhardt, V. Duchatelle, D. Courmoyer, T. Petroni, J. Tanguay, S. Robb, J. Mann, M. Guertin, R.S. Wright, P.L. L'Allier, J. Tardif, Effects of the P-selectin antagonist inlacumab on myocardial damage after percutaneous coronary intervention according to timing of infusion: insights from the SELECT-ACS Trial, *J. Am. Heart Assoc* 5 (2016), <https://doi.org/10.1161/JAHA.116.004255>.
- [63] S. Ferber, G. Tiram, A. Sousa-Herves, A. Eldar-Boock, A. Krivitsky, A. Scomparin, E. Yeini, P. Ofek, D. Ben-Shushan, L.I. Vossen, K. Licha, R. Grossman, S. Ram, J. Henkin, E. Ruppin, N. Auslander, R. Haag, M. Calderón, R. Satchi-Fainaro, Co-targeting the tumor endothelium and P-selectin-expressing glioblastoma cells leads to a remarkable therapeutic outcome, *Elife* 6 (2017), <https://doi.org/10.7554/eLife.25281>.
- [64] Y. Shamay, M. Elkabets, H. Li, J. Shah, S. Brook, F. Wang, K. Adler, E. Baut, M. Scaltriti, P.V. Jena, E.E. Gardner, J.T. Poirier, C.M. Rudin, J. Baselga, A. Haimovitz-Friedman, D.A. Heller, P-selectin is a nanotherapeutic delivery target in the tumor microenvironment, *Sci. Transl. Med* 8 (2016) 345ra87, <https://doi.org/10.1126/scitranslmed.aaf7374>.
- [65] R.I. Mahato, K. Anwer, F. Tagliaferri, C. Meaney, P. Leonard, M.S. Wadhwa, M. Logan, M. French, A. Rolland, Biodistribution and gene expression of lipid/plasmid complexes after systemic administration, *Hum. Gene Ther.* 9 (1998) 2083–2099, <https://doi.org/10.1089/hum.1998.9.14-2083>.
- [66] J. Kisucka, A.K. Chauhan, B.-Q. Zhao, I.S. Patten, A. Yesilaltay, M. Krieger, D. D. Wagner, Elevated levels of soluble P-selectin in mice alter blood-brain barrier function, exacerbate stroke, and promote atherosclerosis, *Blood*. 113 (2009) 6015–6022, <https://doi.org/10.1182/blood-2008-10-186650>.
- [67] R.I. Mahato, K. Kawabata, T. Nomura, Y. Takakura, M. Hashida, Physicochemical and pharmacokinetic characteristics of Plasmidic DNA/ cationic liposome complexes, *J. Pharm. Sci.* 84 (1995) 1267–1271, <https://doi.org/10.1002/jps.2600841102>.
- [68] L.G. Barron, K.B. Meyer, F.C. Szoka, Effects of complement depletion on the pharmacokinetics and gene delivery mediated by cationic lipid–DNA complexes, *Hum. Gene Ther.* 9 (1998) 315–323, <https://doi.org/10.1089/hum.1998.9.3-315>.
- [69] K.L. Brigham, B. Meyrick, B. Christman, M. Magnuson, G. King, L.C. Berry, Rapid communication: in vivo transfection of murine lungs with a functioning prokaryotic gene using a liposome vehicle, *Am J Med Sci* 298 (1989) 278–281, <https://doi.org/10.1097/00000441-198910000-00013>.
- [70] L.G. Barron, L. Gagne, F.C. Szoka, Lipoplex-mediated gene delivery to the lung occurs within 60 minutes of intravenous administration, *Hum. Gene Ther.* 10 (1999) 1683–1694, <https://doi.org/10.1089/10430349950017680>.
- [71] J.W. McLean, E.A. Fox, P. Baluk, P.B. Bolton, A. Haskell, R. Pearlman, G. Thurston, E.Y. Umemoto, D.M. McDonald, Organ-specific endothelial cell uptake of cationic liposome-DNA complexes in mice, *Am. J. Physiol. Circ. Physiol.* 273 (1997) H387–H404, <https://doi.org/10.1152/ajpheart.1997.273.1.H387>.
- [72] P.S. Kowalski, P.J. Zwiers, H.W.M. Morselt, J.M. Kuldo, N.G.J. Leus, M.H. J. Ruijters, G. Molema, J.A.A.M. Kamps, Anti-VCAM-1 SAINT-O-Somes enable endothelial-specific delivery of siRNA and downregulation of inflammatory genes in activated endothelium in vivo, *J. Control. Release* 176 (2014) 64–75, <https://doi.org/10.1016/j.jconrel.2013.12.029>.
- [73] P.S. Kowalski, P.R. Kuinty, K.T. Bijlsma, M.C.A. Stuart, N.G.J. Leus, M.H. J. Ruijters, G. Molema, J.A.A.M. Kamps, SAINT-liposome-polyplex particles, a new carrier for improved delivery of siRNAs to inflamed endothelial cells, *Eur. J. Pharm. Biopharm.* 89 (2015) 40–47, <https://doi.org/10.1016/j.ejpb.2014.11.015>.
- [74] L.S. Uyechi, L. Gagné, G. Thurston, F.C. Szoka, Mechanism of lipoplex gene delivery in mouse lung: binding and internalization of fluorescent lipid and DNA complexes, *Gene Ther.* 8 (2001) 828–836, <https://doi.org/10.1038/sj.gt.3301461>.
- [75] Y. Ito, S. Kawakami, P. Charoensit, Y. Higuchi, M. Hashida, Evaluation of proinflammatory cytokine production and liver injury induced by plasmid DNA/ cationic liposome complexes with various mixing ratios in mice, *Eur. J. Pharm. Biopharm.* 71 (2009) 303–309, <https://doi.org/10.1016/j.ejpb.2008.09.005>.
- [76] J.D. Toussignant, A.L. Gates, L.A. Ingram, C.L. Johnson, J.B. Nietupski, S.H. Cheng, S.J. Eastman, R.K. Scheule, Comprehensive analysis of the acute toxicities induced by systemic Administration of Cationic Lipid:plasmid DNA complexes in mice,

- Hum. Gene Ther. 11 (2000) 2493–2513, <https://doi.org/10.1089/10430340050207984>.
- [77] H. Yoshida, M. Nishikawa, S. Yasuda, Y. Mizuno, H. Toyota, T. Kiyota, R. Takahashi, Y. Takakura, TLR9-dependent systemic interferon- β production by intravenous injection of plasmid DNA/cationic liposome complex in mice, *J. Gene Med.* 11 (2009) 708–717, <https://doi.org/10.1002/jgm.1348>.
- [78] M.A. Yudin, V.N. Bykov, A.S. Nikiforov, R.I. Al-Shekhadat, I.M. Ivanov, T. M. Ustinova, Study of the efficiency of the Hydroporation for delivery of plasmid DNA to the cells on the model of toxic neuropathy, *Bull. Exp. Biol. Med.* 164 (2018) 798–802, <https://doi.org/10.1007/s10517-018-4083-0>.
- [79] B.I. Hudson, A.M. Carter, E. Harja, A.Z. Kalea, M. Arriero, H. Yang, P.J. Grant, A. M. Schmidt, Identification, classification, and expression of RAGE gene splice variants, *FASEB J.* 22 (2008) 1572–1580, <https://doi.org/10.1096/fj.07-9909com>.
- [80] A.Z. Kalea, N. Reiniger, H. Yang, M. Arriero, A.M. Schmidt, B.I. Hudson, Alternative splicing of the murine receptor for advanced glycation end-products (RAGE) gene, *FASEB J.* 23 (2009) 1766–1774, <https://doi.org/10.1096/fj.08-117739>.
- [81] R. López-Díez, A. Rastrojo, O. Villate, B. Aguado, Complex tissue-specific patterns and distribution of multiple RAGE splice variants in different mammals, *Genome Biol. Evol.* 5 (2013) 2420–2435, <https://doi.org/10.1093/gbe/evt188>.
- [82] H. Yonekura, Y. Yamamoto, S. Sakurai, R.G. Petrova, M.J. Abedin, H. Li, K. Yasui, M. Takeuchi, Z. Makita, S. Takasawa, H. Okamoto, T. Watanabe, H. Yamamoto, Novel splice variants of the receptor for advanced glycation end-products expressed in human vascular endothelial cells and pericytes, and their putative roles in diabetes-induced vascular injury, *Biochem. J.* 370 (2003) 1097–1109, <https://doi.org/10.1042/bj20021371>.
- [83] G. Degani, A. Barbiroli, P. Magnelli, S. Digiovanni, A. Altomare, G. Aldini, L. Popolo, Insights into the effects of N-glycosylation on the characteristics of the VC1 domain of the human receptor for advanced glycation end products (RAGE) secreted by *Pichia pastoris*, *Glycoconj. J.* 36 (2019) 27–38, <https://doi.org/10.1007/s10719-018-09855-x>.
- [84] J.V. Geffer, A.L. Shaufli, M.P. Fink, R.L. Delude, Comparison of distinct protein isoforms of the receptor for advanced glycation end-products expressed in murine tissues and cell lines, *Cell Tissue Res.* 337 (2009) 79–89, <https://doi.org/10.1007/s00441-009-0791-0>.
- [85] A. Raucci, S. Cugusi, A. Antonelli, S.M. Barabino, L. Monti, A. Bierhaus, K. Reiss, P. Saftig, M.E. Bianchi, A soluble form of the receptor for advanced glycation endproducts (RAGE) is produced by proteolytic cleavage of the membrane-bound form by the sheddase a disintegrin and metalloprotease 10 (ADAM10), *FASEB J.* 22 (2008) 3716–3727, <https://doi.org/10.1096/fj.08-109033>.
- [86] L. Zhang, M. Bukulin, E. Kojro, A. Roth, V.V. Metz, F. Fahrenholz, P.P. Nawroth, A. Bierhaus, R. Postina, Receptor for advanced Glycation end products is subjected to protein Ectodomain shedding by Metalloproteinases, *J. Biol. Chem.* 283 (2008) 35507–35516, <https://doi.org/10.1074/jbc.M806948200>.
- [87] L. Ramsgaard, J.M. Englert, J. Tobolewski, L. Tomai, C.L. Fattman, A.S. Leme, A. M. Kaynar, S.D. Shapiro, J.J. Enghild, T.D. Oury, The role of the receptor for advanced Glycation end-products in a murine model of silicosis, *PLoS One* 5 (2010), e9604, <https://doi.org/10.1371/journal.pone.0009604>.
- [88] A. Fiszer-Kierzkowska, N. Vydra, A. Wysocka-Wycisk, Z. Kronekova, M. Jarzab, K. M. Lisowska, Z. Krawczyk, Liposome-based DNA carriers may induce cellular stress response and change gene expression pattern in transfected cells, *BMC Mol. Biol.* 12 (2011) 27, <https://doi.org/10.1186/1471-2199-12-27>.
- [89] X.-G. Cai, J.-R. Xia, W.-D. Li, F.-L. Lu, J. Liu, Q. Lu, H. Zhi, Anti-fibrotic effects of specific-siRNA targeting of the receptor for advanced glycation end products in a rat model of experimental hepatic fibrosis, *Mol. Med. Rep.* 10 (2014) 306–314, <https://doi.org/10.3892/mmr.2014.2207>.
- [90] L. Park, K.G. Raman, K.J. Lee, Y. Lu, L.J. Ferran, W.S. Chow, D. Stern, A. M. Schmidt, Suppression of accelerated diabetic atherosclerosis by the soluble receptor for advanced glycation endproducts, *Nat. Med.* 4 (1998) 1025–1031, <https://doi.org/10.1038/2012>.
- [91] T. Burkholder, C. Foltz, E. Karlsson, C.G. Linton, J.M. Smith, Health evaluation of experimental laboratory mice, *Curr. Protoc. Mouse Biol.* 2 (2012) 145–165, <https://doi.org/10.1002/9780470942390.mo110217>.
- [92] E.M.F. Spangenberg, L.J. Keeling, Assessing the welfare of laboratory mice in their home environment using animal-based measures – a benchmarking tool, *Lab. Anim.* 50 (2016) 30–38, <https://doi.org/10.1177/0023677215577298>.
- [93] L. Romero-Castillo, I. Posadas, V. Ceña, Exploring the in vivo toxicity of nanoparticles, *Can. J. Chem.* 95 (2017) 917–926, <https://doi.org/10.1139/cjc-2017-0203>.